DEVELOPMENT OF HIGHLY LUMINESCENT AND WATER-DISPERSIBLE LANTHANIDE-BASED NANOMATERIALS FOR POTENTIAL BIO-MEDICAL IMAGING

A thesis presented to the faculty of the Graduate School of Western Carolina University in partial fulfillment of the requirements for the degree of Master of Science in Chemistry.

By

Gayanthi Kumari Attanayake

Director: Dr. Channa R. De Silva,
Assistant Professor, Inorganic Chemistry,
Department of Chemistry & Physics

Committee Members: Dr. David D. Evanoff, Chemistry
Dr. Carmen L. Huffman, Chemistry

April 2013

ACKNOWLEDGEMENTS

I would like to thank the Department of Chemistry and Physics at Western Carolina University (WCU), Cullowhee, NC, 28723, USA for providing me the opportunity to complete my M.S degree thesis work. I am thankful to my TRAC members Assistant Professor Channa R. De Silva, Assistant Professor David D. Evanoff, and Associate Professor Carmen L. Huffman, for their continuous involvement in the project. I realize that it would not be possible to accomplish this project without the efforts of my TRAC committee. I would like to extend my deepest gratitude to my research advisor, Assistant Professor Channa R. De Silva for his encouragement and spontaneous willingness to answer my numerous questions. I would like to thank our collaborators Professor Romanowski and Mr. Christian Gainer, Department of Biomedical Engineering, Bio5 Institute, University of Arizona, Tucson, AZ, 85719, USA. My sincere thanks goes to Professor David Butcher, Associate Dean of the College of Arts and Sciences at WCU and Associate Professor Cynthia A. Atterholt, Head of the Department of Chemistry and Physics at WCU for their regular support and guidance which helped me to accomplish my M.S. degree successfully and on time. I would like to respectfully thank all the faculty members in the Department of Chemistry and Physics at WCU and thank my friends and family members for their kind cooperation throughout my studies at Western Carolina University.

TABLE OF CONTENTS

LIST OF TABLES

LIST OF FIGURES

LIST OF ABBREVIATIONS

TTA = theonyltrifluoroacetone
AEP = aminoethyl phosphate
HFA = 1,1,1,5,5,5-Hexafluoroacetylacetone
MSH4 = melanocyte stimulating hormone
MC1R = melanocortin-1 receptor
btfa = 4,4,4-Trifluoro-1-pheny-1,3-butandione
XRD = X-ray diffraction
TGA = Thermo Gravimetric Analysis
TEM = Transmission Electron Microscope
SEM = Scanning Electron Microscope
FT-IR = Fourier Transmission Infrared
EDS = energy dispersive X-ray mapping studies

ABSTRACT

DEVELOPMENT OF HIGHLY LUMINESCENT AND WATER-DISPERSIBLE LANTHANIDE-BASED NANOMATERIALS FOR POTENTIAL BIO-MEDICAL IMAGING

Gayanthi Kumari Attanayake

Western Carolina University (April 2013)

Director: Assistant Professor Channa R. De Silva

Lanthanide metal ions exhibit fascinating optical and magnetic properties. Lanthanide-based nanomaterials have potential applications in optical devices, telecommunication, electroluminescent devices, bio-analytical sensors, and bio-medical imaging technology. Despite the recent developments, low luminescence characteristics, poor water solubility, and poor cell selectivity of lanthanide-based materials limit their use in bio-medical applications. This project is designed to mainly improve the luminescence properties of Eu(III)-based nanomaterials for their potential use in biomedical applications. In addition, we explore synthetic methods to enhance the water dispersibility and melanoma cell selectivity of the nanoparticles. Current research is designed to address the above mentioned drawbacks of lanthanide-based nanomaterials. Two different nanoparticle systems were developed in this project. i. europium (Eu)-based down-converting nanoparticles, ii. ytterbium (Yb)- erbium (Er)-based upconverting nanoparticles.

Many down-converting nanoparticle systems suffer from low-luminescence efficiencies due to their poor light absorption by direct excitation of the lanthanide ions.

In order to improve the luminescence characteristics, we have designed a novel nanomaterial by surface-coating it with organic chromophores having strong light absorption properties. $LaEuF_3$.AEP (La=lanthanum, AEP = aminoethyl phosphate) nanoparticles were successfully synthesized using a low temperature heating method and Eu-based $NaYF_4$ nanoparticles were synthesized using a high temperature heating method. A ligand exchange procedure was developed to functionalize the surface of the nanoparticles with an organic chromophore, TTA (thenoyltrifluoroacetone). The TTA functionalized Eu(III)-based nanoparticles exhibit impressive luminescence enhancements utilizing the sensitization effect.

Poor water solubility is the main drawback of the upconverting nanoparticles for bio-medical applications. We have optimized a ligand exchange procedure to functionalize nanoparticle surface by using water soluble and highly coordinative aminoethyl phosphate (AEP) ligand. Water soluble AEP coated Yb- and Er-doped $NaYF_4$ upconverting nanoparticles were prepared using high temperature method.

The synthesized nanoparticles were characterized using UV-visible absorption, Fourier transform infrared (FT-IR), and fluorescence spectroscopic techniques, X-ray powder diffraction (XRD), thermogravimetric analysis (TGA) and electron microscope techniques (TEM and SEM). Luminescent quantum yields of the down-converting nanoparticles were enhanced due to surface modification. The luminescence lifetime studies and luminescence enhancement of the nanoparticles will be discussed with an emphasis on their potential use in biomedical applications.

Our attempts to improve the selectivity of the nanoparticles will be discussed where the nanoparticles were labeled with a melanocortin stimulating hormone (MSH4) peptide ligand targeted to human melanocortin receptors (hMCRs). Once fully developed, the nanoparticle platform has potential use in screening melanoma cancer cell surface-selective biomolecules and *in vivo* imaging of melanoma cancer.

CHAPTER 1

INTRODUCTION

1.1 BACKGROUND

Luminescent nanomaterials in the form of nanoparticles, nanorods, nanowires, nanotubes, as well as colloidal or bulk nanocrystals are of interest for several applications including light emitting diodes, laser technology, telecommunication, sensor applications, cell-based luminescence assays, and medical diagnostics including cancer imaging.[1] Nanomaterials (with nanometer-sized dimensions) have impressive optical properties compared to those observed for their macroscopic materials (millimeter-sized dimensions). This phenomenon increases their recent attention among the scientific community towards nano-biotechnological applications.[2] In recent years, luminescent lanthanide-based nanoparticles have found novel uses in diverse biomedical applications including whole cell binding assays and cancer imaging.[3]

Historically, a wide variety of organic fluorescent reagents including fluorescein and rhodamine has been used as biological labels. These dye molecules have been synthesized with functional terminals for the attachment of selective protein molecules for targeted imaging. Despite the successful use of organic dyes for cellular imaging, organic dyes limit their *in vivo* applications due to broad emission bands, fast photobleaching, and short luminescence lifetimes. Rapid photobleaching of organic dyes (within 10 to 15 minutes) limit their use in time-dependent imaging experiments. Their short fluorescence lifetimes (1-100 ns) correlate with short-lived natural fluorescent

background found in biological samples and limit their use with proteins in the nano-molar binding range.[4]

Luminescent lanthanide metal ions, on the other hand, have many characteristics making them attractive candidates for biological applications. Lanthanide metal ions have well-defined and narrow (line-like) emission bands with large Stokes shifts (up to 300 nm) (Figure 1.1). The unique luminescence characteristics of lanthanide metal ions result from their 4*f* electronic configurations which are shielded by the filled 5*s* and 5*p* sub-shells.[5, 6] Due to large Stokes shifts and narrow emission peaks, lanthanide ions can be used as multi-probes for biological measurements. Lanthanide ions exhibit limited photo-bleaching, higher chemical stability than that of organic dyes and long luminescence lifetimes, mostly in the visible and near infrared regions of the electromagnetic spectrum.[7]

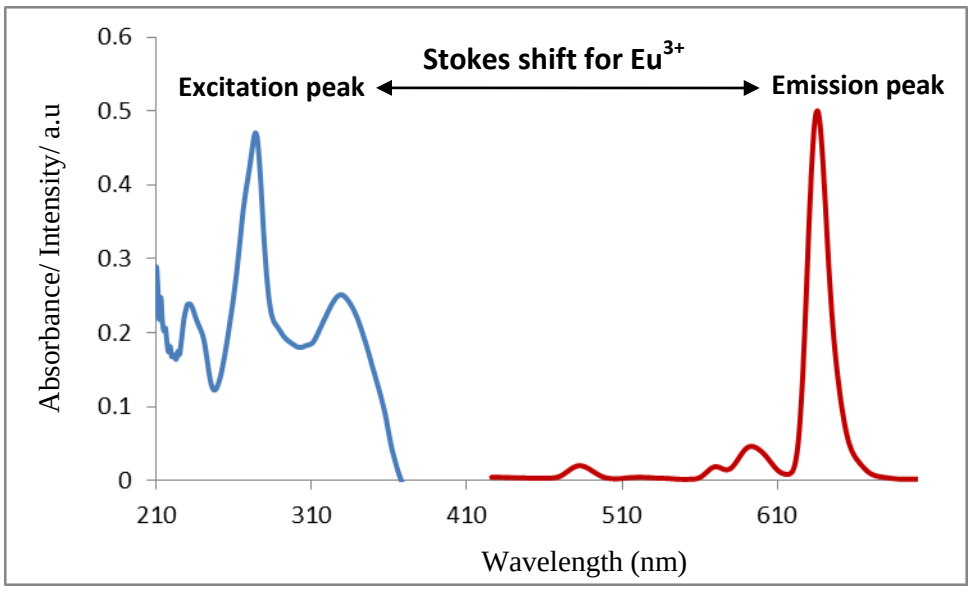

Figure 1.1. Narrow emission peaks and Stokes shift of Eu^{3+} ion.

Longer luminescence lifetimes of lanthanide ions promise a higher signal-to-noise ratio during cell-based luminescence measurements. Short-lived background fluorescence of cellular components, so-called autofluorescence can be rejected by using a delay time during the luminescence detection. This method is known as time-resolved luminescence detection which provides a platform for analyzing nanomolar to picomolar binding agents.

These luminescent features make the lanthanide-based materials useful in *in vivo* and *in vitro* biomedical imaging. For example, synthesis of silica coated $LaVO_4:Eu^{3+}$ core shell nanoparticles have been reported using a high temperature method. Water dispersible silica engineered $LaVO_4:Eu^{3+}$ core shell nanoparticles exhibited good biocompatibility with human lung epithelial H522 cells and PBMC cells. The nanoparticles emit red luminescence (614 nm) upon UV excitation at 273 nm.[8]

Lanthanide chelator-doped nanoparticles have also been utilized for binding assays. For example, polystyrene beads with a diameter of 107 nm containing Eu(III)–2-thenoyl- trifluoroacetone complexes were coated with streptavidin. This assay protocol provided high sensitivity with a 100-fold increase of luminescence over the conventional assay methods using Eu-labeled streptavidin. However, polystyrene nanoparticles have limitations for their use in cell-based binding assays including the larger particle size, swelling, and leakage of the encapsulated Eu-chelator molecules through surface defects.

A new class of lanthanide materials, so-called upconverting nano-phosphors (UNPs), has recently been developed for use in biomedicine. These nanomaterials emit visible light upon near infrared excitation (NIR). Current high temperature synthetic

methods produce nanomaterials with hydrophobic coatings. Most of the biological applications require hydrophilic UNPs with high upconverting luminescence efficiency. To this end, poly(vinylpyrrolidone) coated Gd/Yb/Er co-doped $NaYF_4$ nanocrystals have been prepared with diameters of 40-100 nm using a one-pot solvothermal synthesis method.[9] According to the literature reports, these nanoparticles exhibit the most efficient upconverting luminescence at 546 and 668 nm (upon excitation at 980 nm).[9] Another class of nanomaterials exhibits NIR-to-NIR (near infrared) upconversion process which provides deeper light penetration into a biological specimen and results in high contrast optical imaging due to the absence of an autofluorescence background and minimum light scattering upon NIR excitation. Water-dispersible fluoride ($NaYF_4$) nanocrystals (with a particle diameter of 20-30 nm) co-doped with Tm^{3+} and Yb^{3+} ions were used for NIR-based imaging.[10] *In vitro* cellular uptake of this class of nanoparticles was visualized using the characteristic emission of Tm^{3+} at 800 nm excited with 975 nm. $NaYF_4$ nanocrystals co-doped with Tm^{3+} and Yb^{3+} ions were intravenously injected into mice with no observed cytotoxicity. These nanoparticles demonstrated high contrast *in vivo* imaging in mice using upconversion photoluminescence.[10]

Notwithstanding the current progress using lanthanide-based nanomaterials in biotechnology, luminescence generation is very difficult by direct excitation of the lanthanide ions due to their poor ability to absorb light. This weak light absorption is caused by the parity (Laporte) forbidden nature of the 4*f* electronic transitions resulting in very weak luminescence.[11] In addition, poor water solubility and poor cell-selective targeting limit their use in biomedical applications. Most of the literature-reported

lanthanide nanoparticles are hydrophobic and face great challenges in effective imaging of cancer cells and tissues. This project is designed to address the above three problems, especially the low luminescence efficiencies of lanthanide-based nanoparticles.

1.2 INTRODUCTION TO RESEARCH

This research project was designed to address the limitations discussed in the background section. We have designed synthetic methods to develop nanomaterials with improved photoluminescence and water-dispersibility. The work is focused on two main different types of lanthanide-based nanoparticles:

(a) europium-based down-converting nanoparticles

i) $LaEuF_3$: synthesized using low temperature method

ii) $Eu:NaYF_4$: synthesized using high temperature method

Europium-based nanoparticles will be developed to improve the luminescence characteristics, hydrophilicity of the nanoparticle surface, and the selectivity of nanoparticles to melanoma cancer cell-surface receptors.

(b) ytterbium-, and erbium-based ($Yb:Er: NaYF_4$) upconverting nanoparticles.

$Yb:Er:NaYF_4$ upconverting nanoparticles will be designed to improve the hydrophilicity of the nanoparticle surface and the selectivity of nanoparticles to melanoma cancer cell-surface receptors.

1.2.1 Upconverting Nanoparticles

Upconversion refers to the process where excitation is carried out with low energy photons [usually near-infrared (NIR)] resulting in the emission of high energy photons (visible).[12] This phenomena is made possible in lanthanides due to multiple metastable electronic states. Upconverting lanthanide nanoparticles consist of two components, an inorganic host lattice and dopant ions that are capable of upconverting. The transparent crystalline host lattice is chosen to be $NaYF_4$ which can accommodate trivalent lanthanide ions with multiple metastable excited states. Ytterbium (Yb^{3+}) has a high absorption coefficiency (in the NIR region) that can increase upconversion efficiency. In the upconversion system Yb^{3+} acts as the absorber, taking the lower energy photons from the excitation source, and energy will be transferred to erbium (Er^{3+}) which acts as the emitter. Er^{3+} emits high energy photons (in the visible region) as shown in Figure 1.2.[12]

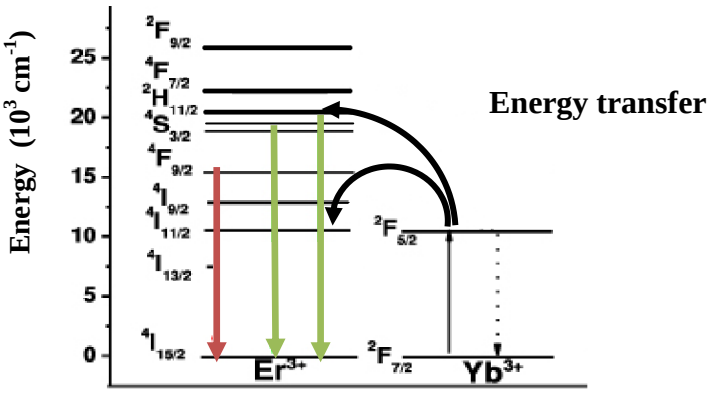

Figure 1.2. Upconversion mechanism in the Yb^{3+} and Er^{3+} doped $NaYF_4$ nanoparticle system.[12]

Many literature reported upconverting nanoparticles exhibit a sharp emission bandwidth, long luminescence lifetime, high photostability, and low cytotoxicity, which render them particularly useful in bio-medical imaging applications.[13] Upconverting nanoparticles are typically prepared in the presence of a hydrophobic capping ligand (such as oleic acid) that controls the particle growth and stabilizes the particles against aggregation in solution.[14] In this project we optimized a synthetic method to replace the hydrophobic capping ligands on the surface with a hydrophilic ligand using a ligand exchange reaction. The ligand exchange method can be used with a wide variety of hydrophilic organic molecules such as aminoethyl phosphate (AEP) (Figure 1.3).[15,16] Water soluble AEP coated $NaYF_4$: Yb^{3+}, Er^{3+} nanoparticles can efficiently be dispersed in biological media for imaging applications.

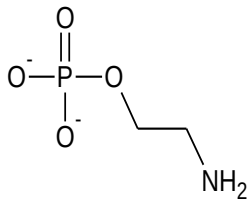

Figure 1.3. Structure of aminoethyl phosphate.

1.2.2 Europium-based Down-converting Lanthanide Nanoparticles

Europium-based nanoparticles can be utilized for biomedical imaging through their energy down-conversion process. In down-conversion process the excitation is carried out using high-energy photons resulting in an emission of low-energy photons (Figure 1.4).[17]

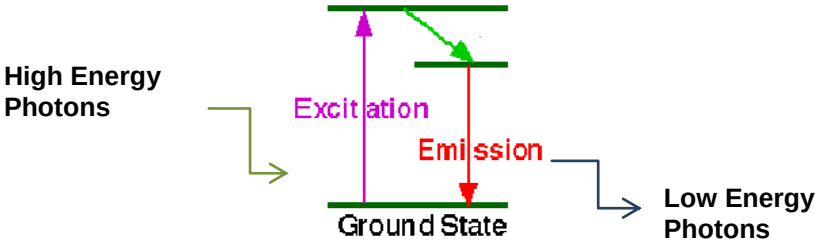

Figure 1.4. Energy down-conversion process.

Among different lanthanide metals, europium shows red emission in a nanocrystal with an emission wavelength of 615 nm ($^5D_0 \longrightarrow {}^7F_2$ electronic transition) as shown in Figure 1.5.[17,18] Several research groups designed Eu-based nanoparticles that are suitable of cellular imaging. For example, Eu_2O_3 (europium oxide),[19] EuF_3 (europium fluoride),[19] and $EuPO_4$ (europium phosphate)[19] nanoparticles have been developed with red emission characteristics. It has also been demonstrated that the nanoparticles can be attached to protein molecules for studying protein-protein interactions.[19]

The main drawback of europium-based down-converting lanthanide nanoparticles is the weak absorption of light. We believe that the poor light absorption can be overcome by using a surface-coated chromophore ligand. A chromophore ligand with efficient light absorption properties can be attached to the surface of the lanthanide-based nanoparticles. The chromophore acts as an "antenna" which absorbs light and transfers energy to lanthanide-based excited states for an efficient luminescence. This process is known as "sensitization" of lanthanide metal ions by an organic molecule and is represented schematically in Figure 1.6A.[18]

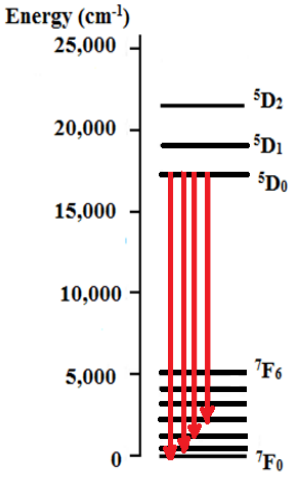

Figure 1.5. Electronic energy-level diagram of the europium ion (Eu^{3+}).

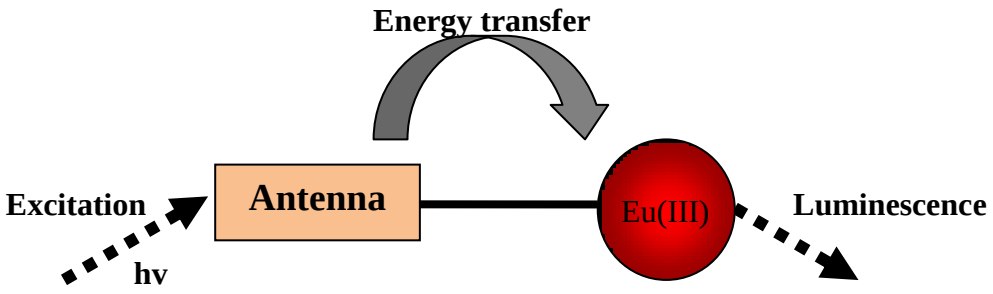

(A)

Figure 1.6 (A). Schematic representation of the sensitization process.

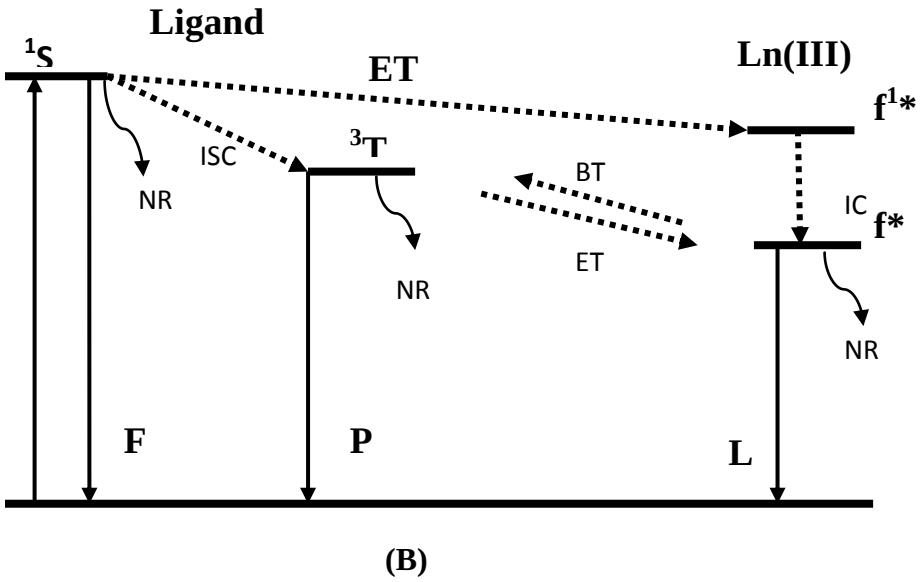

Figure 1.6 (B). Schematic representation of lanthanide-centered luminescence.[20,21]

In Figure 1.6B, ^{1}S and ^{3}T are the ligand-based singlet and triplet states, which can decay by fluorescence (F) or phosphorescence (P) processes, respectively, or through non-radiative (NR) pathways. ISC is inter-system crossing between the two states and energy transfer (ET) leads to population of the Ln(III)-based excited states (f*). The excited state of the Ln(III) decays by radiative pathways [luminescence (L)] to produce lanthanide-centered luminescence. BT is the back-energy transfer which may happen if the triplet state of the ligand and the excited states of the metal ions are close in energy.[20] Lanthanide-centered luminescence is efficient if the ligand-based singlet and triplet energies are matched with the lanthanide-based excited states. The structural parameters also play a role in energy transfer as the distance between the antenna and the metal ion is crucial for an efficient energy transfer process.[21]

The sensitization process has been widely used in lanthanide chelators to improve the luminescence properties. For example, europium complexes featuring fluorinated β-diketonate ligands such as thenoyltrifluoroacetone (TTA), 4,4,4-trifluor-1phenyl-1,3-butanedione (btfac), nitrogen *p,p'*-disubstituted bipyridine (dmbipy), and dimethyl phenanthroline (dmphen) were synthesized.[22] UV excitation of these complexes led to red luminescence characteristics of the Eu(III) ion. These chelator compounds exhibit impressive quantum yield values (25% to 35%). For example, $Eu(TTA)_3(dmbipy)$ (Figure 1.7) exhibited red luminescence with a quantum yield value of 23%.[23]

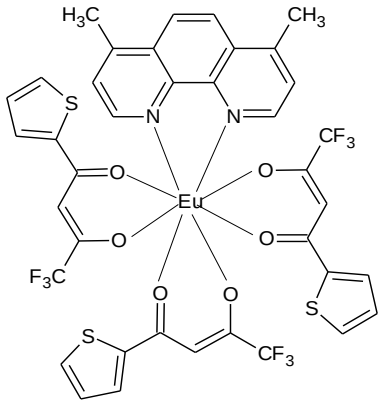

Figure 1.7. Molecular structure of $Eu(TTA)_3(dmphen)$.

However, a sensitization phenomenon is currently not well developed for lanthanide-based nanoparticle systems. Some sensitized lanthanide nanoparticles exhibit very low quantum yield values. For example, LaEuF3-AEP (AEP = aminoethyl phosphate) nanoparticles were sensitized with the 6-carboxy-5'-methyl-2.2'-bipyridine ($bipyCOO^-$) ligand (Figure 1.8). These nanoparticles exhibited a luminescence quantum yield value of 2.8%.[11]

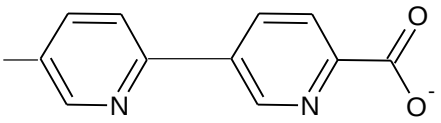

Figure 1.8. Structure of bipyCOO$^-$ ligand.

Hypothesis: We hypothesized that the sensitization of Eu-based nanoparticles with fluorinated oxygen-donor ligands will significantly enhance the luminescence properties of the nanoparticles suitable for *in vitro* cancer imaging with a high signal-to-noise ratio.

In this project, we have chosen to use a class of organic ligands known as "β-diketonates" which are very efficient chromophores for the sensitization of europium(III) ions based on the above mentioned chelation chemistry. We plan to improve the luminescence efficiency of the nanoparticles using β-diketonate ligands, namely 4,4,4-trifluoro-1-(2-thienyl)-1,3-butandione (TTA), 1,1,1,5,5,5-hexafluoroacetylacetone (HFA), and 4,4,4-trifluoro-1-pheny-1,3-butanedione (btfa)[22,23] (Figure 1.9a,1.9b,1.9c) as the surface functionalization agents. Initial Eu-doped LaF_3 (lanthanum fluoride) nanoparticles will be prepared using a low temperature method utilizing aminoethyl phosphate (AEP) as the surface stabilization agent.[11] In addition to using the AEP ligand we plan to use other water soluble ligands including citric acid and mercaptopropionic acid (Figure 1.9d and 1.9e) to further explore different surface functionalizing ligands for improved water dispersibility of nanoparticles.[15] The surface of these nanoparticles will then be functionalized with the TTA ligand for improved luminescence properties.

A schematic representation of the proposed ligand exchange protocol is depicted in Figure 1.10.

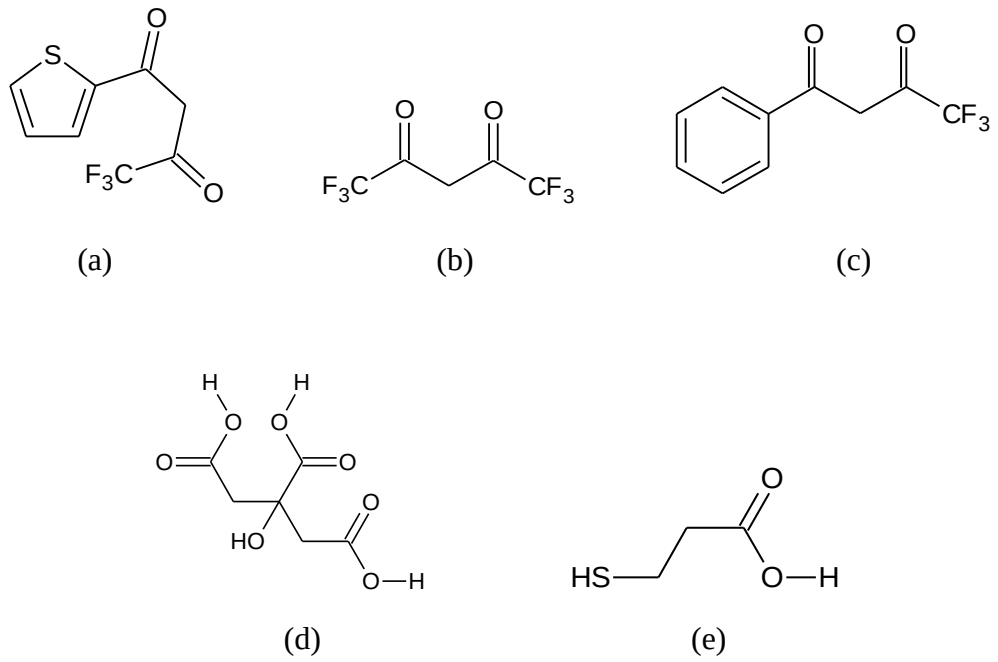

Figure 1.9. Structures of (a) 4,4,4-trifluoro-1-(2-thienyl)-1,3-butandione (TTA) (b) 1,1,1,5,5,5-hexafluoroacetylacetone (HFA) (c) 4,4,4-trifluoro-1-pheny-1,3-butanedione (btfa) (d) citric acid and (e) mercaptopropionic acid.

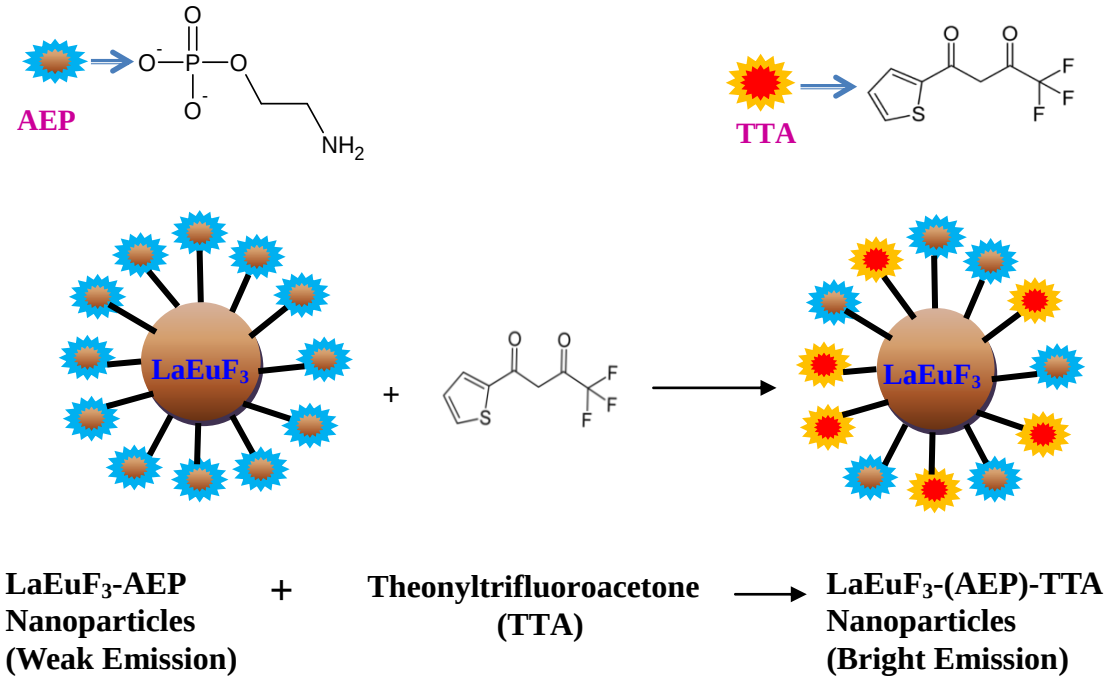

Figure 1.10. Surface functionalization of AEP coated $LaEuF_3$ nanoparticles with TTA chromophore.

Eu(III)-doped $NaYF_4$ nanoparticles will be prepared using a high temperature decomposition method using oleic acid ($CH_3(CH_2)_7CH=CH(CH_2)_7COOH$) (Figure 1.11) as the stabilization agent. Hydrophobic oleic acid can be removed using an acid treatment protocol[24] and the TTA ligand can then be introduced to Eu:$NaYF_4$ nanoparticles system as shown in Figure 1.12.

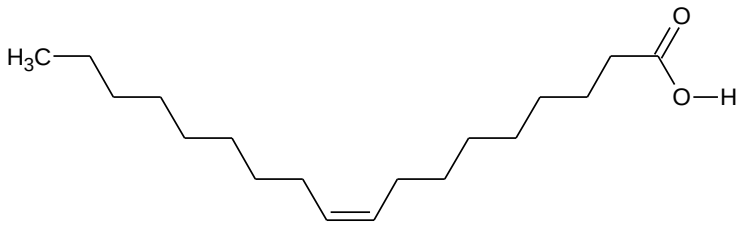

Figure 1.11. Molecular structure of oleic acid.

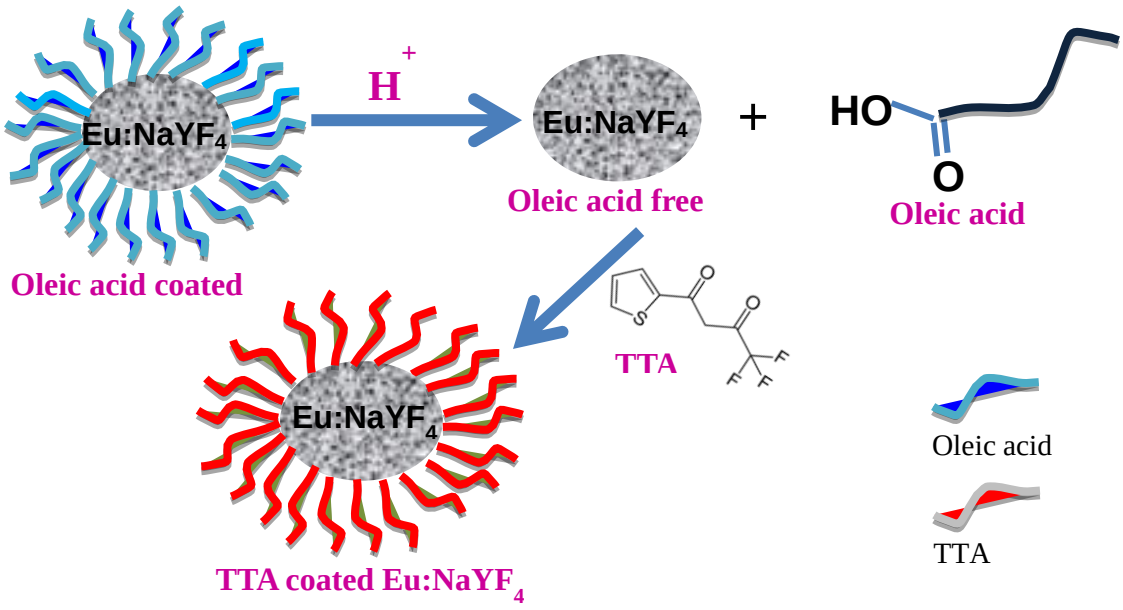

Figure 1.12. Surface functionalization of Eu:$NaYF_4$ nanoparticles with the TTA ligand.

Both upconverting and europium-based down-converting nanoparticles will be labeled with melanocyte stimulating hormone (MSH4) peptide. This can be done through the carboxylic-amino coupling between the peptide and the AEP ligand. MSH4 is a small peptide which contains four amino acid residues. Those 4 amino acids are histidine (His), *D*-phenylalanine (*D*-Phe), arginine (Arg), and tryptophan (Trp) (Figure 1.13). MSH4 selectively binds to the human melanocortin receptor system which belongs to a type of G-protein coupled receptor (GPCR) family. It has been recently reported that human melanocrotin-1 receptor (MC1R) is more abundant in melanoma cancer cells than those observed in normal melanoma cells.[25] A linker based on polyethylene glycol (known as PEG-20) will be attached to the MSH4 hormone to minimize any binding interferences due to the presence of the nanoparticle.

MSH4-labeled nanoparticles can be utilized for selective imaging of melanoma cancer cells (Figure 1.14).

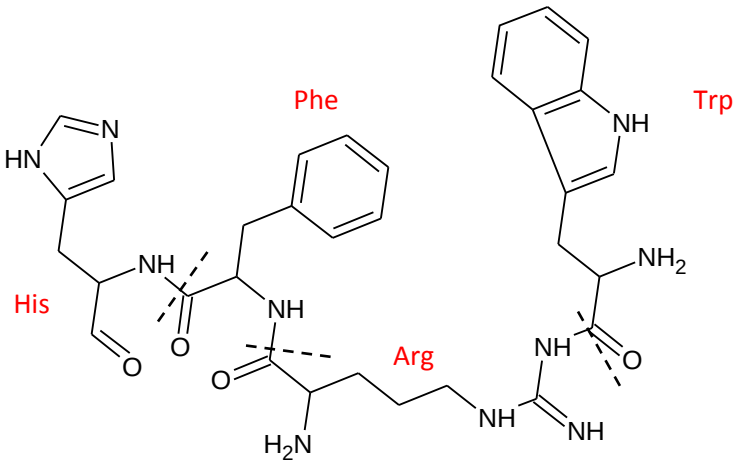

Figure 1.13. Structure of MSH4 peptide (His-*D*-Phe-Arg-Trp).

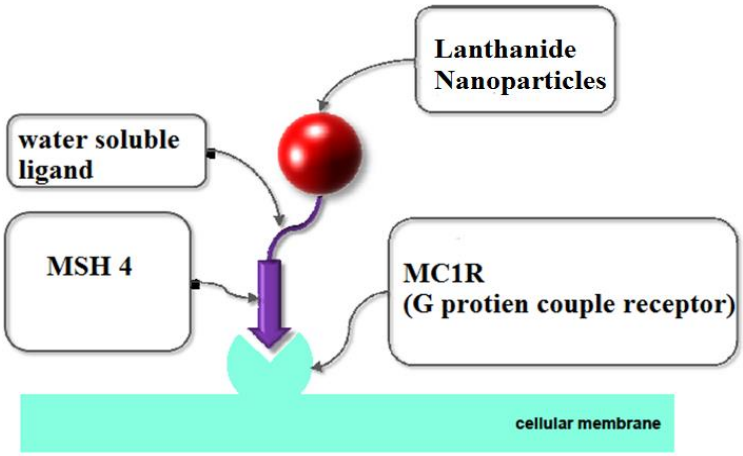

Figure 1.14. Schematic representation of ligand receptor coupling between MC1R receptor and MSH4-labeled nanoparticles.

CHAPTER 2

EXPERIMENTAL

2.1 MATERIALS AND INSTRUMENTATION

All the reagents were purchased from Aldrich or Fisher Scientific. The reagents were used without further purification. Nanopure water with a resistivity of 18.2MΩ was obtained from a Barnstead NANOpure Diamond system with a 0.2μm hollow fiber filter.

2.1.1 Fourier Transform Infrared Spectroscopy

Fourier transform infrared (FT-IR) spectra were collected using a Perkin-Elmer Spectrum One spectrometer. Solid samples were vacuumed dried before mounting on the stage of the FT-IR instrument. Spectra were collected using Spectrum One software at a resolution of 4 cm^{-1} with 16 scans averaged per spectrum in the range of 400 - 4000 cm^{-1}.

2.1.2 Absorption Spectroscopy

Ultraviolet (UV) visible spectra were recorded on an Agilent 8453 UV-visible Spectrometer. Samples were prepared by dispersing 0.1 mg of the nanoparticle samples in 2 mL of the solvent (water or water:ethanol (1:1 (v/v)). Samples were sonicated for 15 minutes at room temperature before collecting the spectra. The absorption spectra were collected from 200 nm to 900 nm using quartz cuvettes.

2.1.3 Luminescence Spectroscopy

Luminescence spectra were collected using a Perkin Elmer LS-55 fluorescence spectrometer with a 5 nm slit width using quartz cuvettes. Samples were prepared by

dispersing 0.1 mg of the nanoparticle samples in 2 mL of the solvent (water or water:ethanol 1:1 (v/v)). The samples were sonicated for 15 minutes at room temperature before collecting spectra. The samples were excited at 340 nm and the emission spectra were collected from 200 nm to 700 nm using a scan speed of 200 nm/minute.

2.1.4 X-ray Powder Diffraction Studies

Solid samples were grounded and mounted on the XRD well plate. X-ray powder diffraction spectra were collected using a desktop X-ray diffractometer "MiniFlex^{+}", with a Cu-Kα (λ = 1.5418 A˚) radiation and a scan speed of 0.5° min^{-1}. Diffraction data were collected from 2θ = 3˚ to 2θ = 80˚. The X-ray generator was set at a power of 30 kV with a current of 40 mA. X-ray diffraction data were analyzed using Materials Data Jade 7 software.

2.1.5 Thermogravimetric Analysis

Thermogravimetric analyses were conducted using a Perkin Elmer Diamond Differential Thermal Analyzer with 20 mL min-1 N_2 purge. Dry solid powders were used to collect spectra. The temperature was set to ramp from 50 ˚C to 600 ˚C at a temperature ramp of 5˚C min^{-1}. Onset option and X, Y tangents of the Pyris program were used to determine the mass loss points. Delta Y option was used to calculate the mass percentages.

2.1.6 Transmission Electron Microscopy (TEM) & Scanning Electron Microscopy (SEM) Studies

Size and the shape of the nanoparticles were determined using a TEM 9500 microscope with an operating voltage of 300 kV and a STEM-Hitachi HD2000 microscope operating at 200 kV. Samples were prepared by making a dispersion of nanoparticles (1 mg nanoparticles / 1mL solvent) and drop casting 200 μL of the sample on a carbon coated copper grid (300 mesh). Samples were dried at room temperature by natural solvent evaporation.

2.1.7 Luminescence Lifetime Measurements

Luminescence lifetime measurements of the nanoparticles were carried out using a photomultiplier tube (Hamamatsu R928) coupled to a 500 MHz band pass digital oscilloscope (Tektronix TDS 620B). Excitation was provided by a tunable optical parametric oscillator (OPO) pumped by a Nd:YAG laser Q-switched at 20 Hz with a 3 ns pulse width.

2.2 EUROPIUM BASED DOWN-CONVERTING NANOPARTICLES (LOW TEMPERATURE METHOD)

2.2.1 Preparation of $LaEuF_3$-AEP Nanoparticles

$LaEuF_3$-AEP nanoparticles were synthesized using AEP, lanthanide (III) salts and sodium fluoride at pH 6.5 using a literature procedure[11] with slight modifications.

Briefly, AEP (4 mmol, 675 mg) was dissolved in argon purged nanopure water (35 mL). The pH of the solution was adjusted to 6.5 by drop-wise addition of a 28% aqueous ammonia solution. The reaction solution was heated to 75 °C while magnetic stirring. A mixture of $LaCl_3.7H_2O$ (1.1 mmol, 444 mg) and $Eu(NO_3)_3.5H_2O$ (0.13 mmol, 56 mg) in methanol (2 mL) was added drop-wise to the AEP solution. Then, NaF (3.1 mmol, 130 mg) in water (2 mL) was added drop-wise to the stirring solution. The clear reaction mixture was stirred for 2 hours at 75 °C with periodic argon purging (Figure 2.1). Ethanol (80 mL) was added to precipitate the nanoparticles (a white powder). The nanoparticles were isolated by centrifugation (3000 rpm, 20 min), washed with ethanol (10 mL), and dried at room temperature.

2.2.2 Preparation of $LaEuF_3$-(AEP)-TTA Nanoparticles

$LaEuF_3$-AEP nanoparticles (75 mg) were dispersed in water (3 mL). The solution of TTA (0.12 mmol, 16 mg) and triethylamine (0.14 mmol, 15 µL) in water (2 mL) was added drop-wise to the stirring reaction solution. The solution was stirred for 2 hours at room temperature (Figure 2.2). The product was isolated by centrifugation (3000 rpm, 10 min). A series of $LaEuF_3$-(AEP)-TTA nanoparticles was prepared by changing the amount of TTA ligand (64 mg (0.48 mmol), 32 mg (0.24 mmol), 16 mg (0.12 mmol), 8 mg (0.06 mmol), and 4 mg (0.03 mmol)).

2.2.3 Preparation of $LaEuF_3$-(AEP)-HFA Nanoparticles

$LaEuF_3$-(AEP)-HFA nanoparticles were prepared using 1,1,1,5,5,5-hexafluoroacetylacetone (HFA) (0.096 mmol, 16 mg) and preparative procedures

identical to those used to synthesize $LaEuF_3$-(AEP)-TTA nanoparticles. The product was isolated by centrifugation (3000 rpm, 10 min).

2.2.4 Preparation of $LaEuF_3$-Mercaptopropionic Acid Nanoparticles

$LaEuF_3$-mercaptopropanoic acid nanoparticles were synthesized using mercaptopropionic acid (6.36 mmol, 675 mg), lanthanide (III) salts and sodium fluoride at pH 6.5 and preparative procedures identical to those used to synthesize $LaEuF_3$-AEP nanoparticles.

2.2.5 Preparation of $LaEuF_3$-Citric Acid Nanoparticles

$LaEuF_3$-citric acid nanoparticles were synthesized using citric acid (9.5 mmol, 2 g) and preparative procedures identical to those used to synthesize $LaEuF_3$-AEP nanoparticles.

2.2.6 Preparation of $LaEuF_3$-(Citric Acid)-TTA Nanoparticles

$LaEuF_3$-(citric acid)-TTA nanoparticles were prepared using $LaEuF_3$-citric acid nanoparticles (75 mg), TTA (0.12 mmol, 16 mg) and preparative procedures identical to those used to synthesize $LaEuF_3$-(AEP)-TTA nanoparticles.

2.3 EUROPIUM BASED DOWN-CONVERTING NANOPARTICLES (HIGH TEMPERATURE METHOD)

2.3.1 Preparation of Oleic Acid Coated Eu:$NaYF_4$ Nanoparticles

Lanthanide trifluoroacetate precursors ($Ln(TFA)_3(H_2O)_2$) (Figure 2.1) (Equation 1) were prepared using europium oxide (Eu_2O_3), yttrium oxide (Y_2O_3) and trifluoroacetic

acid (99%). Eu_2O_3 (10 mol %, 0.125 mmol, 43 mg) and Y_2O_3 (90 mol %, 1.125 mmol, 250 mg) were dissolved in a solution mixture of trifluoroacetic acid (5 mL) and nanopure water (5 mL). This reaction solution was refluxed at 80 °C. The residual water and acid were then slowly evaporated to dryness at 50 °C. Lanthanide trifluoroacetate precursors were isolated using a rotary evaporator.

$$CF_3COOH_{(aq)} + Ln_2O_{3\,(s)} \longrightarrow Ln(TFA)_3(H_2O)_{2\,(s)} \quad (1) \qquad Ln = Eu^{3+}, Y^{3+}$$

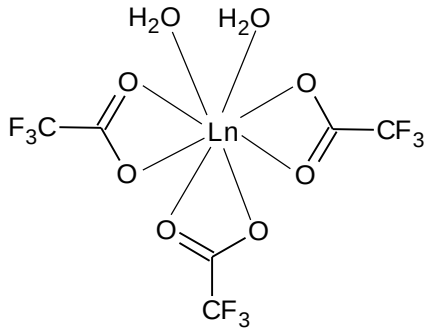

Figure 2.1. Structure of a lanthanide trifluoroacetate precursor.

$$Ln(TFA)_3(H_2O)_{2(s)} + NaTFA_{(s)} + \text{oleic acid}_{(aq)} + \text{octadecane}_{(aq)} \xrightarrow{280\ ^0C} Eu{:}NaYF_{4(s)} \quad (2)$$

Lanthanide TFA precursors and sodium TFA (NaTFA) (2.5 mmol, 340 mg) were added to the reaction vessel with oleic acid (90%, 20 mL) and octadecane (90%) (20 mL) (Equation 2). The resulting solution was slowly heated to 100 °C under vacuum with magnetic stirring for 30 minutes to remove residual water and oxygen during which the flask was purged periodically with dry argon gas. The resulting clear solution had a slight yellow color. The solution was then heated to 300 °C at an approximate rate of

10 °C/ min under dry argon and kept at this temperature for 1 hour. At approximately 250 °C, the evolution of small gas bubbles was observed from the solution indicating the decomposition of the metal trifluoroacetate precursors. A burst of nucleation was observed between 280-300 °C which resulted in the solution becoming turbid. Subsequently, the mixture was allowed to cool to room temperature during which time the solution became clear and a yellow colloidal suspension was obtained. The nanocrystals were precipitated by the addition of hexane/acetone (v/v 1:4) and isolated via centrifugation (3000 rpm, 10 min). The resulting nanoparticle pellet was washed once with ethanol (10 mL) and further purified by dispersing in a minimum amount of hexane and precipitating with excess ethanol. The resulting pellet was subsequently washed with acetone and isolated via centrifugation (3000 rpm, 10 min).[24]

2.3.2 Preparation of Oleic Acid Free Eu:$NaYF_4$ Nanoparticles

Oleic acid coated Eu:$NaYF_4$ nanoparticles (100 mg) were dispersed in nanopure water (10 mL). The reaction was performed with stirring for 2 h while maintaining the pH at 4 by adding a solution of 0.1 M HCl. During this reaction the carboxylate groups of the oleate ligand were protonated to yield oleic acid. After the reaction was complete, the aqueous solution was mixed with diethyl ether to remove the oleic acid by liquid-liquid extraction. The extraction was carried out three times and the combined ether layers were re-extracted with water. In addition, the water layers were combined and reextracted with diethyl ether. The nanoparticles in the water dispersible fraction were recuperated by centrifugation (3000 rpm, 10 min) after precipitation with acetone.[24]

2.3.3 Preparation of TTA Coated Eu:$NaYF_4$ Nanoparticles

TTA coated Eu:$NaYF_4$ nanoparticles were prepared using TTA (0.12 mmol, 16 mg), oleic acid free Eu:$NaYF_4$ nanoparticles (75 mg) and preparative procedures identical to those used to synthesize $LaEuF_3$-(AEP)-TTA nanoparticles. A series of TTA coated Eu:$NaYF_4$ nanoparticles was prepared by using different amounts of TTA ligand (64 mg (0.48 mmol), 32 mg (0.24 mmol), 16 mg (0.12 mmol), 8 mg (0.06 mmol)).

2.3.4 Preparation of btfa Coated Eu:$NaYF_4$ Nanoparticles

The btfa coated Eu:$NaYF_4$ nanoparticles were prepared using btfa (0.11 mmol, 16 mg), oleic acid free Eu:$NaYF_4$ nanoparticles (75 mg) and preparative procedures identical to those used to synthesize $LaEuF_3$-(AEP)-TTA nanoparticles.

2.3.5 Preparation of Oleic Acid Free Eu:$NaYF_4$-MSH4 Nanoparticles

Eu:$NaYF_4$-MSH4 nanoparticles were prepared using MSH4 (0.15 mmol, 16 mg), oleic acid free Eu:$NaYF_4$ nanoparticles (75 mg) and preparative procedures identical to those used to synthesize $LaEuF_3$-(AEP)-TTA nanoparticles.

2.3.6 Preparation of TTA Coated Eu:$NaYF_4$-MSH4 Nanoparticles

TTA coated Eu:$NaYF_4$-MSH4 nanoparticles were prepared using TTA (0.12 mmol, 16 mg), oleic acid free Eu:$NaYF_4$-MSH4 nanoparticles (75 mg) and preparative procedures identical to those used to synthesize $LaEuF_3$-(AEP)-TTA nanoparticles.

2.4 UPCONVERTING NANOPARTICLES

2.4.1 Preparation of Oleic Acid Coated Yb:Er:$NaYF_4$ Nanoparticles

Oleic acid coated Yb:Er:$NaYF_4$ nanoparticles were prepared using Yb_2O_3 (0.25 mmol, 98.5 mg), Er_2O_3 (0.025 mmol, 9.6 mg), Y_2O_3 (0.975 mmol, 220.2 mg) and preparative procedures identical to those used to synthesize oleic acid coated Eu:$NaYF_4$ nanoparticles.

2.4.2 Preparation of Oleic Acid Free Yb:Er:$NaYF_4$ Nanoparticles

Oleic acid free Yb:Er:$NaYF_4$ nanoparticles were prepared using oleic acid coated Yb:Er:$NaYF_4$ nanoparticles (100 mg) and preparative procedures identical to those used to synthesize oleic acid free Eu:$NaYF_4$ nanoparticles.

2.4.3 Preparation of AEP Coated Yb:Er:$NaYF_4$ Nanoparticles

AEP coated Yb:Er:$NaYF_4$ nanoparticles were prepared using AEP (0.11 mmol, 16 mg), oleic acid free Yb:Er:$NaYF_4$ nanoparticles (75 mg) and preparative procedures identical to those used to synthesize $LaEuF_3$-(AEP)-TTA.

2.5 MATERIALS CHARACTERIZATION

Nanoparticles were characterized by UV-visible, infrared (FT-IR), and fluorescence spectroscopic techniques, transmission electron microscopy (TEM), scanning electron microscopy (SEM), thermogravimetric analysis (TGA), and X-ray powder diffraction (XRD). Luminescence quantum yields (ϕ) of the nanoparticles were calculated using cresyl violet acetate as the reference (ϕ_R = 54 % in methanol)[23] as shown

in Equation (3) where *Abs*, *A* and *n* denote the absorbance (at highest absorption maxima), integrated area of the emission spectrum, and the refractive index of the solvent, respectively. Subscripts *R* and *S* refer to the reference and the sample, respectively. [23]

$$\phi_S = \phi_R \frac{(Abs_R)}{(Abs_S} \frac{(A_s)}{(A_R)} \frac{(n^2_S)}{(n^2_R)} \quad \text{———} \quad (3)$$

Quantum yield measurements were carried out using three different concentrations of the nanoparticles. Each measurement was repeated three times. This procedure was repeated three times in three different days and the average quantum yield value was calculated using the 27 measurements.

Nanoparticle size was determined using a modified Sheerer equation and XRD data. The Sheerer equation (Equation 4) was developed to calculate the nano-crystallite size (*L*) by XRD radiation of wavelength (λ) (Cu Kα = 0.154 nm) from measuring the full width at half maximum of peaks (β) in radians located at any 2θ in the XRD pattern. The shape factor (*K*) can range from 0.62 to 2.08 and is usually taken to be about 0.89. However, if all of the peaks of a pattern are going to give a similar value of *L*, then βcosθ must be identical.

$$L = \frac{K\lambda}{\beta.\cos\theta} \quad \text{———} \quad (4)$$

In a plot of lnβ vs ln(1/cosθ), the intercept of a least squares regression is $K\lambda/L$. This can be used to obtain the nanoparticle size, *L*.[26]

Nanoparticle size distribution was determined using a bitmap picture of the TEM image. By calculating the number of pixels for each nanoparticle, the average particle diameter can be evaluated. The area for the luminescence spectra was calculated using OriginLab data analysis and graphing software.

CHAPTER 3

RESULTS AND DISCUSSION

Our research is planned to prepare three different types of lanthanide nanoparticles to address their limitations for biological applications. The limitations include poor water dispersibility, poor luminescence characteristics, and selectivity. This research project is focused on three different types of nanoparticles:

I. $LaEuF_3$ nanoparticles – low temperature method
II. Eu-$NaYF_4$ nanoparticles – high temperature method

} Eu-based down-converting nanoparticles

III. Yb-Er-$NaYF_4$ upconverting nanoparticles

3.1. TTA COATED $LaEuF_3$-AEP NANOPARTICLES (EUROPIUM-BASED DOWN-CONVERTING NANOPARTICLES: LOW TEMPERATURE METHOD)

Our results obtained for europium-based down-converting nanoparticles are discussed herein. In our modified preparation, the AEP ligand in $LaEuF_3$-AEP nanoparticles was exchanged with the TTA ligand in water to yield TTA coated $LaEuF_3$-(AEP)-TTA nanoparticles. $LaEuF_3$-AEP nanoparticles are readily dispersible in water. After treatment with TTA, a pink color precipitate was observed due to the hydrophobic nature of the surface-coated TTA ligand. $LaEuF_3$-(AEP)-TTA nanoparticles show bright red luminescence upon excitation using a portable UV lamp as opposed to faint emission

observed from the $LaEuF_3$-AEP nanoparticles. The brightest luminescence was observed for the nanoparticles where 32 mg of TTA was used for the exchange reaction.

3.1.1 Fourier Transform Infrared Studies

FT-IR spectra of the free ligand TTA, $LaEuF_3$-AEP, and $LaEuF_3$-(AEP)-TTA nanoparticles were obtained for the dried powders as shown in Figure 3.1(A). The FT-IR spectrum of $LaEuF_3$-AEP nanoparticles has a characteristic peak for the phosphate group around 1080 cm^{-1}. The peak around 2900 cm^{-1} can be assigned to N-H stretching. This confirms the presence of the surface coating AEP ligand. We confirm a successful surface functionalization with TTA ligand by evaluating the carbonyl (C=O) stretching frequency of the TTA ligand. The carbonyl (C=O) stretching frequency in $LaEuF_3$-(AEP)-TTA nanoparticles was shifted from 1640 cm^{-1} (Free TTA) to 1600 cm^{-1} (Figure 3.1(B)).

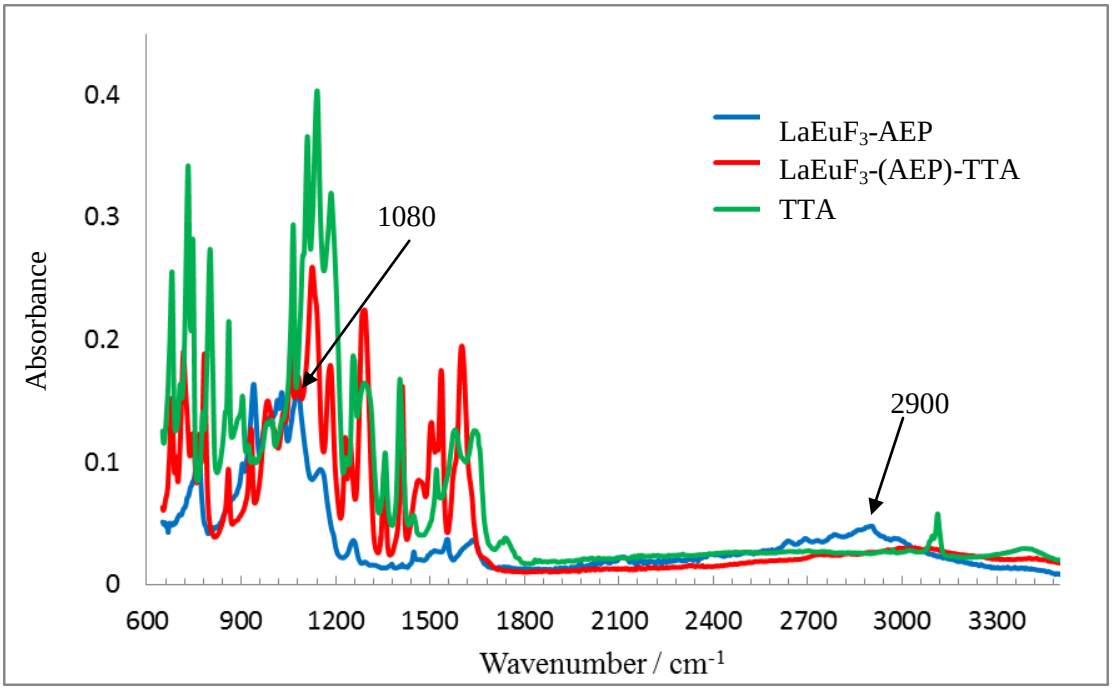

Figure 3.1(A). FT-IR spectra of TTA, $LaEuF_3$-AEP and $LaEuF_3$-(AEP)-TTA nanoparticles.

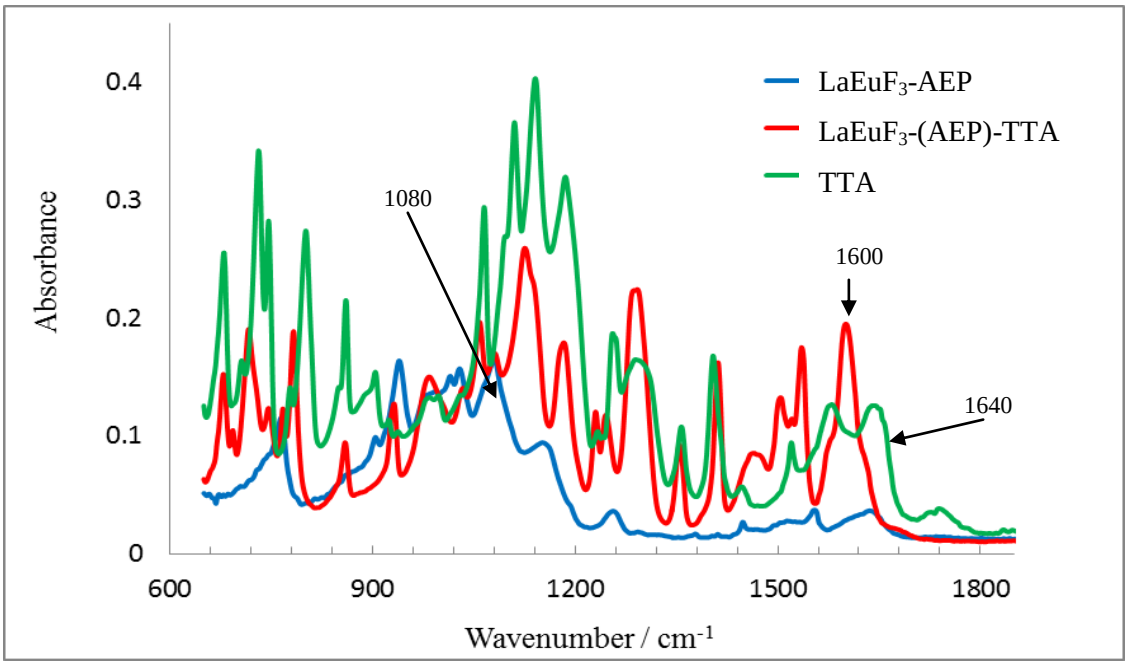

Figure 3.1(B). Fingerprint region of the FT-IR spectra of TTA, $LaEuF_3$-AEP and $LaEuF_3$-(AEP)-TTA nanoparticles.

3.1.2 UV-visible Absorption and Luminescence Studies

TTA attachment to the nanoparticle surface was further confirmed by UV-Vis absorption spectroscopy (Figure 3.2). The change in the UV-visible spectrum from $LaEuF_3$-AEP to $LaEuF_3$-(AEP)-TTA nanoparticles is due to the absorption properties of the newly introduced TTA ligand providing a chromophore for efficient light absorption. A characteristic absorbance maximum at around 343 nm was evident after TTA exchange which matches a characteristic absorption peak in pure TTA ligand.

Figure 3.2 depicts the intense red luminescence of $LaEuF_3$-(AEP)-TTA nanoparticles with an emission maximum at 614 nm due to the $^5D_0$ to $^7F_2$ electronic transition. Collecting a luminescence spectrum of $LaEuF_3$-AEP nanoparticles (before ligand exchange with TTA) was not successful due to its weak luminescence characteristics. Relatively higher concentration of $LaEuF_3$-AEP nanoparticles were required to obtain a luminescence spectrum. This observation provides evidence for our proposed sensitization process resulting in improved luminescence upon TTA ligand exchange.

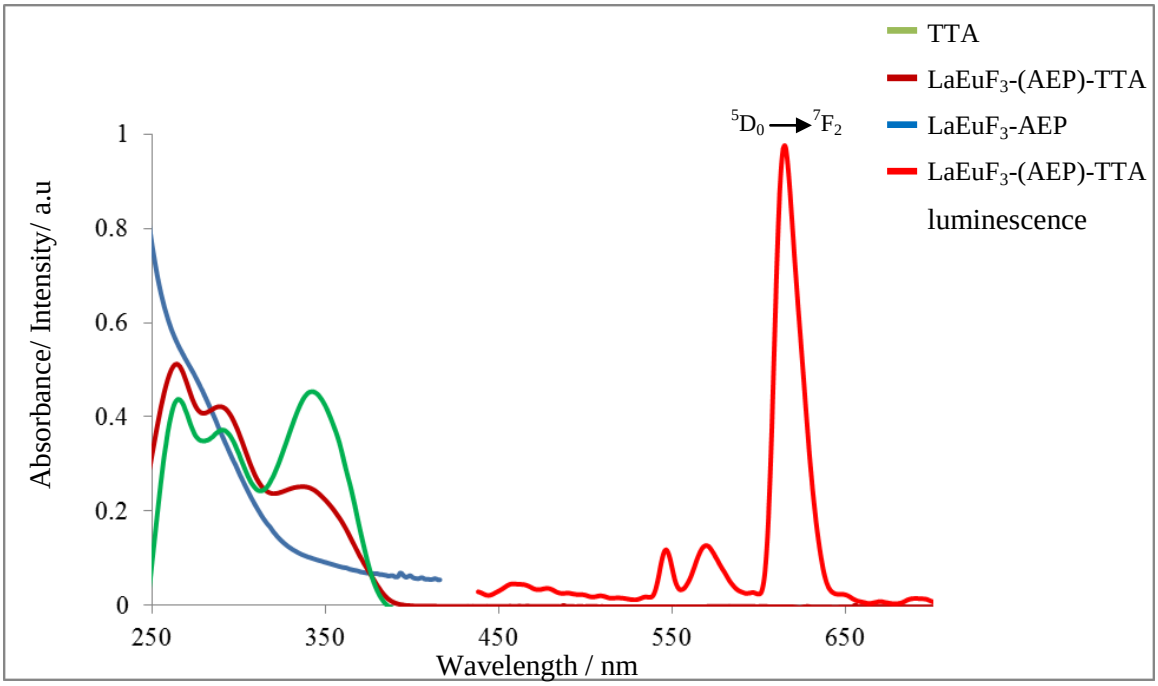

Figure 3.2. UV-visible absorption spectra of $LaEuF_3$-AEP (dispersed in water) and $LaEuF_3$-(AEP)-TTA nanoparticles (dispersed in a water / methanol solution) and luminescence spectrum of $LaEuF_3$-(AEP)-TTA nanoparticles (excited at 343 nm).

3.1.3 X-Ray Powder Diffraction Studies

X-Ray powder diffraction (XRD) patterns of the nanoparticles are shown in Figure 3.3. The XRD peaks observed at 2θ values of 24°, 27°, 43°, and 50.5° confirm the hexagonal structure of LaF_3 nanoparticles. The broad peaks indicate the low crystallinity of the nanoparticles due to the use of a relatively low temperature during the synthesis. Due to the low crystallinity and broader XRD peaks, Use of the Sheerer equation was not successful in determining the size of the $EuLaF_3$ nanoparticles. No significant change in the crystal structure of the nanoparticles was observed after the ligand exchange process according to Figure 3.3(A) and 3.3(B).

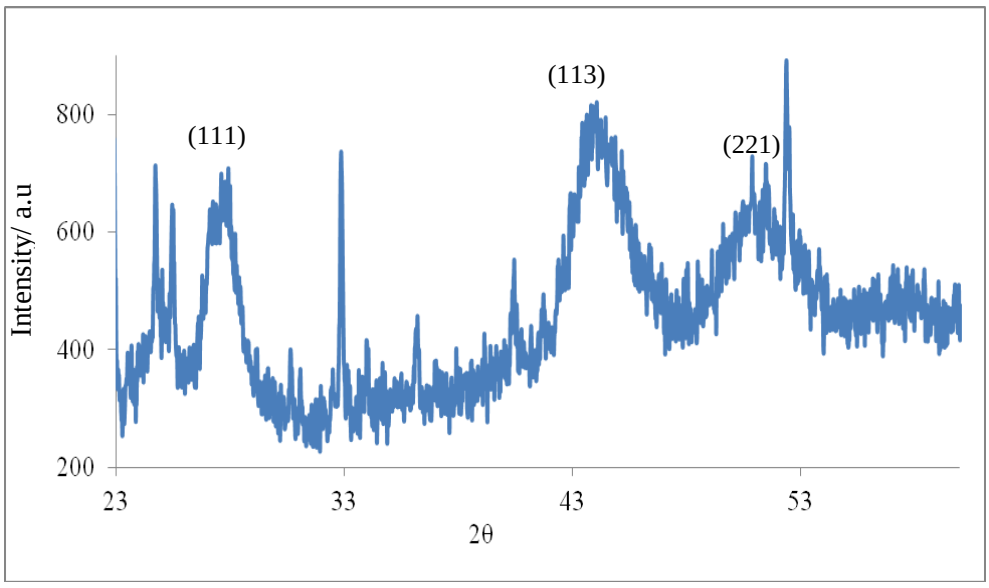

(A)

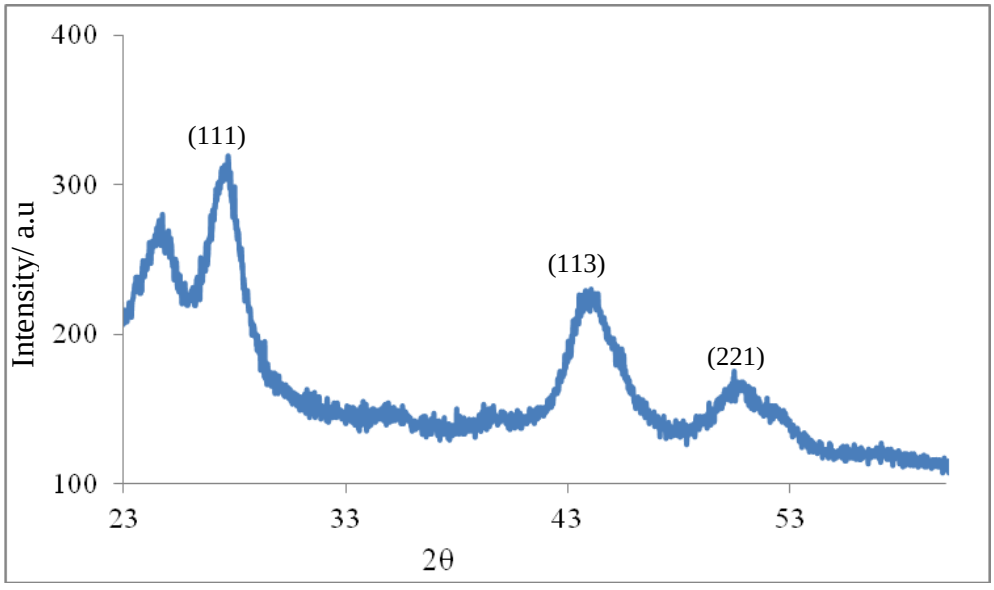

(B)

Figure 3.3. X-ray powder diffraction (XRD) pattern of (A) $LaEuF_3$-AEP and (B) $LaEuF_3$-(AEP)-TTA nanoparticles.

3.1.4 Luminescent Lifetime Measurements

According to Figure 3.4 $LaEuF_3$-AEP nanoparticles show a luminescence lifetime of 900 µs whereas the lifetime of $LaEuF_3$-(AEP)-TTA nanoparticles is 650 µs. No significant change in the lifetimes was observed using direct excitation of Eu(III) ions (465 nm) and TTA excitation (350 nm). $LaEuF_3$-AEP nanoparticles showed a relatively higher luminescence lifetime than that of $LaEuF_3$-(AEP)-TTA nanoparticles. This may be due to the quenching of the luminescence due to a non-radiative decay process in the presence of the TTA ligands. When compared with the luminescence lifetimes of organic dyes (observed in the ns time scale), the lanthanide nanoparticles have relatively higher lifetimes. A Long luminescence lifetime warrants sensitive imaging and cell-based binding assays with a standard 400 µs delay time.

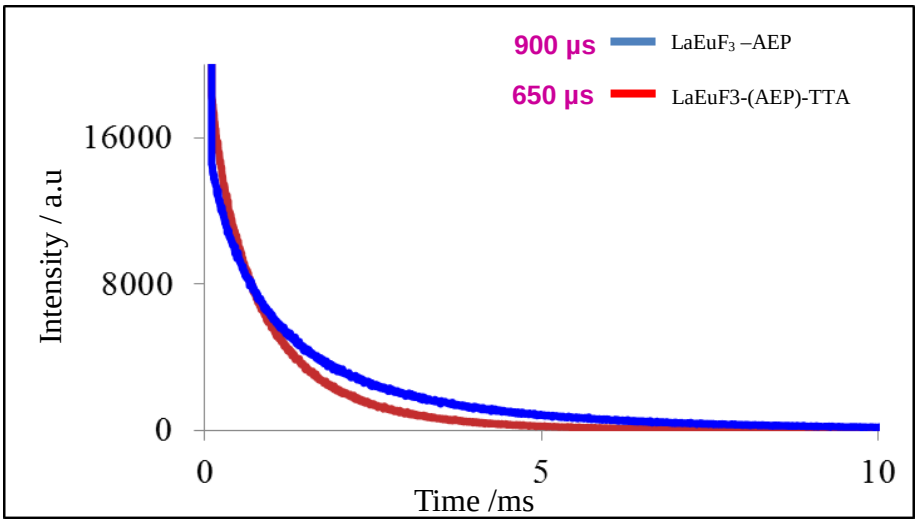

Figure 3.4. Lifetime measurements of $LaEuF_3$-AEP and $LaEuF_3$-(AEP)-TTA nanoparticles.

3.1.5 Transmission Electron Microscope (TEM) Studies

TEM images of $LaEuF_3$-(AEP)-TTA nanoparticles are shown in Figure 3.5. The diameters of the spherical nanoparticles are found to be 100-150 nm. The lattice fringes confirm the crystallanity of the nanoparticles with a lattice spacing of 3.117 Å. The size of the nanoparticles may be too large for *in vivo* biological applications. In this project we are considering melanoma skin cells with an approximate size of 30 μm.[27] When we consider this cell size, these nanoparticles may penetrate through skin cells. However, there may be difficulties in filtering the nanoparticles through the kidney cells due to their large size.

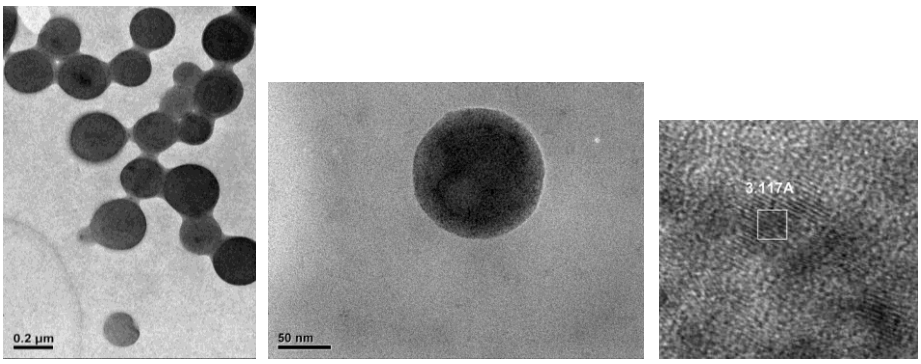

(a) (b) (c)

Figure 3.5. Transmission electron microscope images of (a) $LaEuF_3$-(AEP)-TTA nanoparticles (b) a single nanoparticle and (c) the lattice structure of the nanoparticles.

3.1.6 Thermogravimetric Analysis

TGA diagram of $LaEuF_3$-AEP nanoparticles (Figure 3.6(A)) exhibited one mass loss at 218 °C. This mass loss is assigned to the removal of AEP ligand. TGA diagrams of $LaEuF_3$-(AEP)-TTA nanoparticles (Figure 3.6(B), (C), (D), (E)) exhibit two mass losses. The mass loss at 218 °C is consistence with the mass loss observed in the TGA diagram of $LaEuF_3$-AEP (Figure 3.6(A)) nanoparticles. This mass loss is assigned to the removal of AEP ligand. According to these observations we confirm the presence of AEP ligand in all types of $LaEuF_3$ nanoparticles. In addition, another mass loss at 155 °C, 137 °C, 127 °C and 124 °C was observed for $LaEuF_3$-(AEP)-TTA nanoparticles using 8 mg, 16 mg, 32 mg, and 64 mg of TTA ligand, respectively. This mass loss is assigned to the removal of TTA ligands. Onset option and X, Y tangents of the TGA program were used to find the temperature range and the mass of the curve points. The mass percentages of TTA ligand in different nanoparticles were calculated using delta Y and step options.

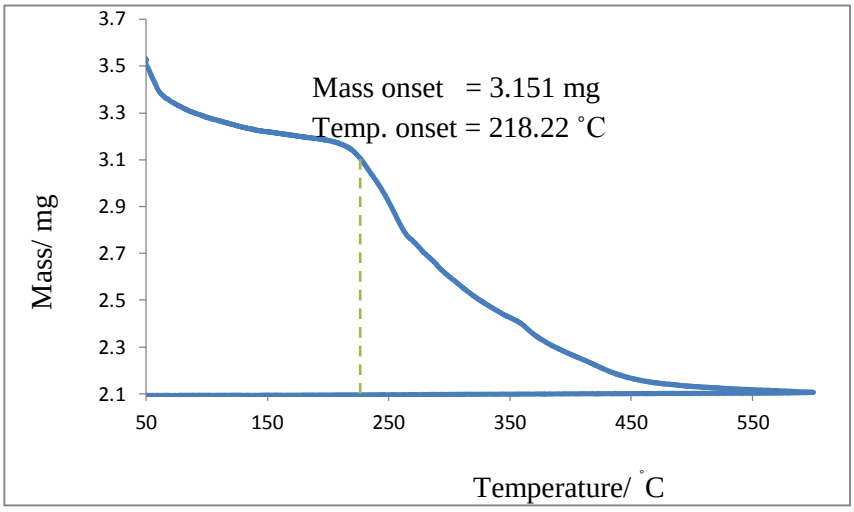

(A)

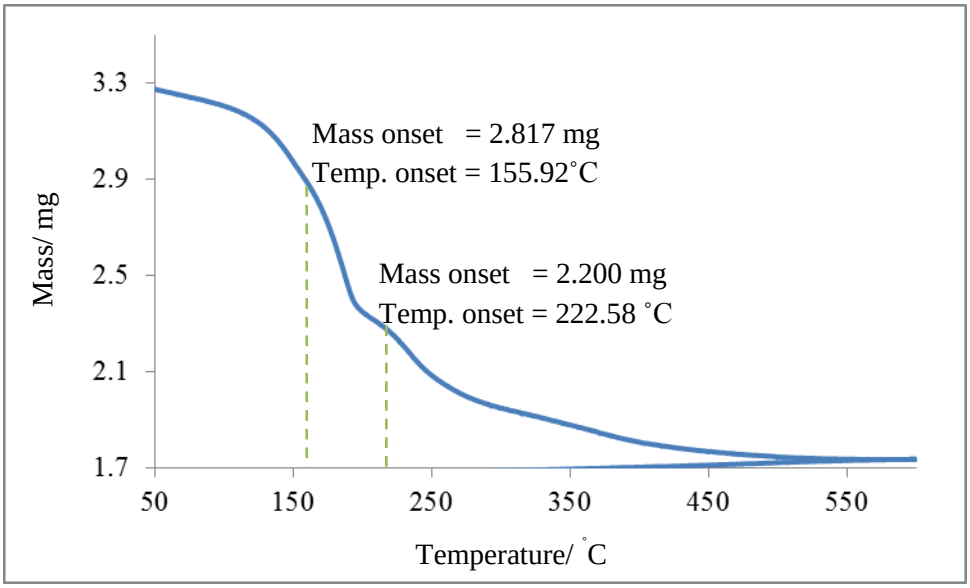

(B)

Figure 3.6. Thermogravimetric analysis of (A) $LaEuF_3$-AEP and (B) $LaEuF_3$-(AEP)-TTA (8 mg) nanoparticles.

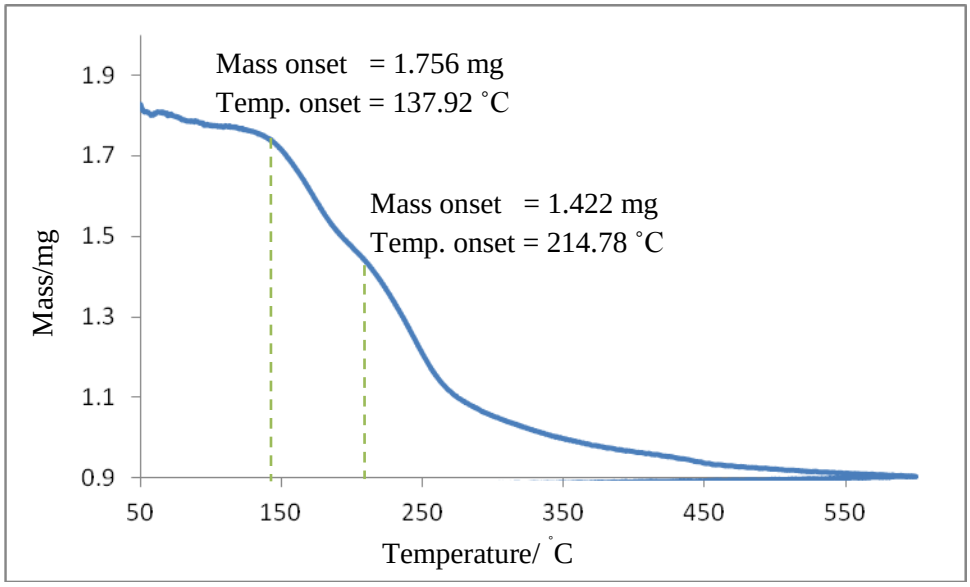

(C)

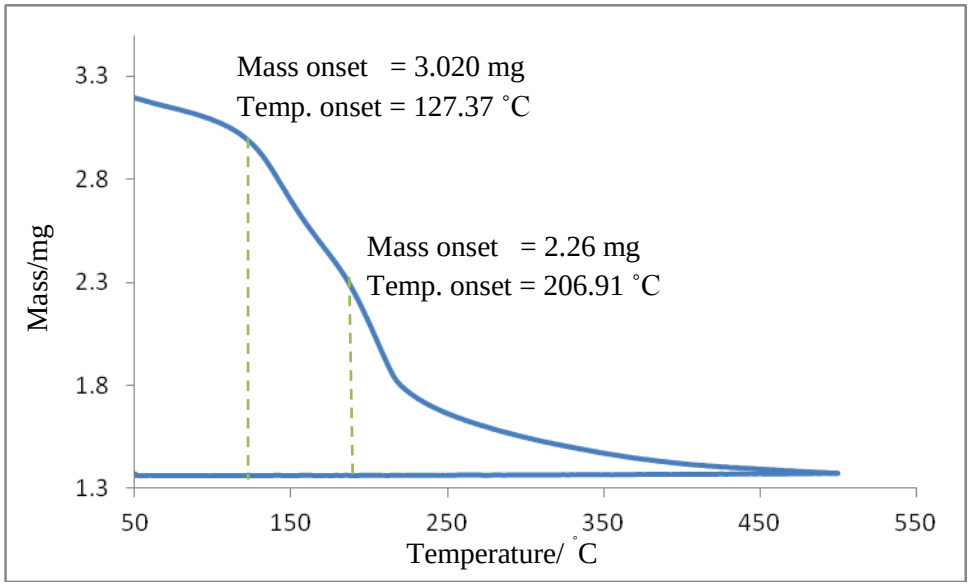

(D)

Figure 3.6. Thermogravimetric analysis of (C) $LaEuF_3$-(AEP)-TTA (16 mg) and (D) $LaEuF_3$-(AEP)-TTA (32 mg) nanoparticles.

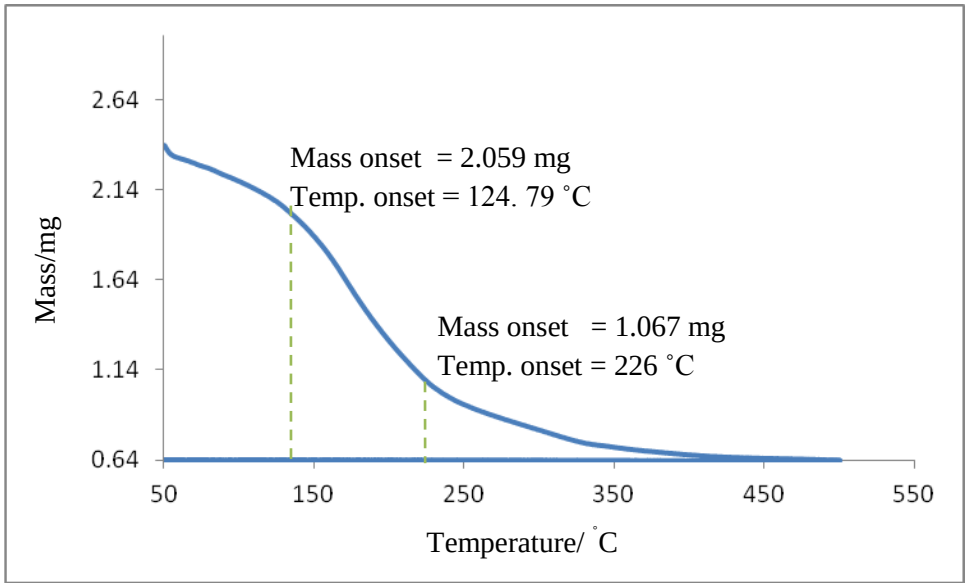

(E)

Figure 3.6. Thermogravimetric analysis of (E) $LaEuF_3$-(AEP)-TTA (64 mg) nanoparticles.

Table 3.1. (A). Mass percentages of TTA in $LaEuF_3$-(AEP)-TTA nanoparticles (using delta Y option)

Nanoparticles	Mass percentage of TTA (%)	Mass percentage of AEP (%)
$LaEuF_3$-(AEP)-TTA (8 mg)	13.72	20.30
$LaEuF_3$-(AEP)-TTA (16 mg)	17.52	19.63
$LaEuF_3$-(AEP)-TTA (32 mg)	38.05	11.73
$LaEuF_3$-(AEP)-TTA (64 mg)	41.38	12.80

Table 3.1 (B). Mass percentages of TTA in $LaEuF_3$-(AEP)-TTA nanoparticles (using step option)

Nanoparticles	Mass percentage of TTA (%)	Mass percentage of AEP (%)
$LaEuF_3$-(AEP)-TTA (8 mg)	6.77	25.77
$LaEuF_3$-(AEP)-TTA (16 mg)	10.69	19.51
$LaEuF_3$-(AEP)-TTA (32 mg)	20.06	13.28
$LaEuF_3$-(AEP)-TTA (64 mg)	19.21	15.91

According to Table 3.1(A) TTA percentage of $LaEuF_3$-(AEP)-TTA nanoparticles varies with the TTA amount used in the synthesis. The highest TTA percentages, 38% and 41% were observed for the nanoparticles where we used 32 mg and 64 mg of TTA ligand, respectively. We can assume that the highest TTA coverage of $LaEuF_3$-(AEP)-TTA nanoparticles is within 38% and 41%. $LaEuF_3$-(AEP)-TTA (32 mg) and $LaEuF_3$-(AEP)-TTA (64 mg) nanoparticles exhibit the highest observed luminescence quantum yield. These results are consistence with the observed TTA percentages. AEP percentage was decreased when we increase the TTA amount. The lowest AEP mass percentage was observed for $LaEuF_3$-(AEP)-TTA (32 mg) nanoparticles. Based on these observations we confirm the ligand exchange process between TTA and AEP.

3.1.7 Luminescence Quantum Yields

Luminescence quantum yields provide a quantitative comparison of the observed luminescence among the various surface functionalized nanoparticles. Table 3.2 shows the calculated relative quantum yields of the nanoparticles studied in this project. $LaEuF_3$-AEP nanoparticles show a very low luminescence quantum yield of 0.0009 %. As was predicted, an impressive enhancement of luminescence quantum yield was observed for the TTA exchanged nanoparticles. The highest quantum yield of 4.0 % was observed for the nanoparticles after using 32 mg of TTA ligand for the exchange process. This value is 1,000 times higher than the $LaEuF_3$-AEP nanoparticles (before the exchange process). The standard deviation of the luminescence quantum yield values was calculated using Microsoft Excel software. Luminescence intensity is directly proportional to the amount of TTA used during the synthesis. Improved luminescence intensities were evident at all levels of TTA exchange compared to the luminescence observed for the $LaEuF_3$-AEP nanoparticles. Figure 3.7 illustrates the luminescence enhancement of the nanoparticles upon TTA coating.

Figure 3.7. Photoluminescence of TTA-uncoated (left) and TTA-coated $LaEuF_3$-AEP nanoparticles (right) (The nanoparticles were excited using a portable UV lamp at 365 nm).

Table 3.2. Luminescence quantum yield values of the prepared $LaEuF_3$-(AEP)-TTA nanoparticles.

Nanoparticles	ϕ	Standard Deviation
$LaEuF_3$-AEP	0.0009%	0.000012
$LaEuF_3$-(AEP)-TTA (4 mg)	0.3%	0.093
$LaEuF_3$-(AEP)-TTA (8 mg)	0.4%	0.082
$LaEuF_3$-(AEP)-TTA (16 mg)	1.0%	0.102
$LaEuF_3$-(AEP)-TTA (32 mg)	4.0%	0.091
$LaEuF_3$-(AEP)-TTA (64 mg)	3.9%	0.124

3.2 TTA COATED $LaEuF_3$-Citric Acid NANOPARTICLES (EUROPIUM-BASED DOWN-CONVERTING NANOPARTICLES: LOW TEMPERATURE METHOD)

Citric acid is another type of water soluble ligand which can be used as a surface coating ligand for lanthanide nanoparticles. Citric acid coated $LaEuF_3$ nanoparticles were reacted with TTA chromophore to produce TTA-coated nanoparticles.

3.2.1 UV-visible Absorption and Luminescence Studies

The UV-visible spectrum of $LaEuF_3$-(Citric acid)-TTA nanoparticles (Figure 3.8(A)) shows a characteristic peak at 343 nm which corresponds to the TTA ligand absorption. The luminescence spectrum of $LaEuF_3$-(Citric acid)-TTA (Figure 3.8(B)) exhibited the characteristic peak of Eu(III) ions at 614 nm.

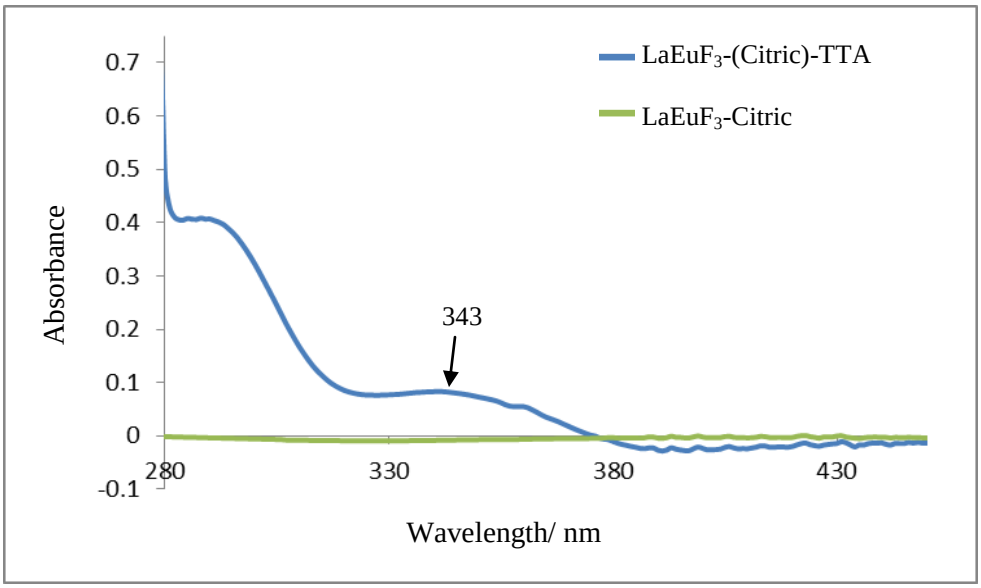

(A)

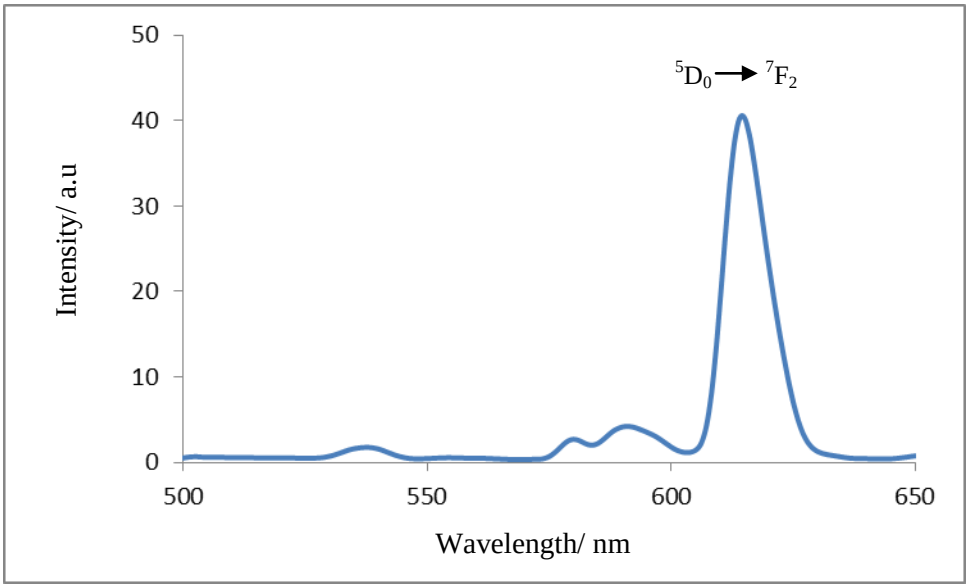

(B)

Figure 3.8. (A) UV-visible absorption spectrum and (B) luminescence spectrum (excited at 343 nm) of $LaEuF_3$-(Citric)-TTA nanoparticles (dispersed in a water / methanol solution).

The quantum yield values of $LaEuF_3$-(Citric)-TTA (16 mg) and $LaEuF_3$-(Citric)-TTA (32 mg) nanoparticles are 1.7% and 1.9% respectively. The calculated relative quantum yield of $LaEuF_3$-(Citric)-TTA (32 mg) (1.9%) nanoparticles was lower than that observed for $LaEuF_3$-(AEP)-TTA (32 mg) (4%) nanoparticles. We assumed that AEP ligands can easily be removed from the nanoparticle surface during the ligand exchange process compared to the removal of citric acid ligands. Citric acid ligand may be tightly bound to the nanoparticle surface via the carboxylic groups. Therefore more TTA ligands can be exchanged with AEP ligands than with the citric acid ligands. This results a higher quantum yield value of 4 % for the $LaEuF_3$-(AEP)-TTA nanoparticles.

3.2.2 X-Ray Powder Diffraction Studies

The same peak positions of XRD pattern of $LaEuF_3$-(AEP)-TTA (Figure 3.3(B)) were observed for $LaEuF_3$-(Citric)-TTA nanoparticles (Figure 3.9) as well. XRD pattern of $LaEuF_3$-(Citric)-TTA confirmed the same crystal structure (hexagonal) of LaF_3 which was observed for $LaEuF_3$-AEP nanoparticles.

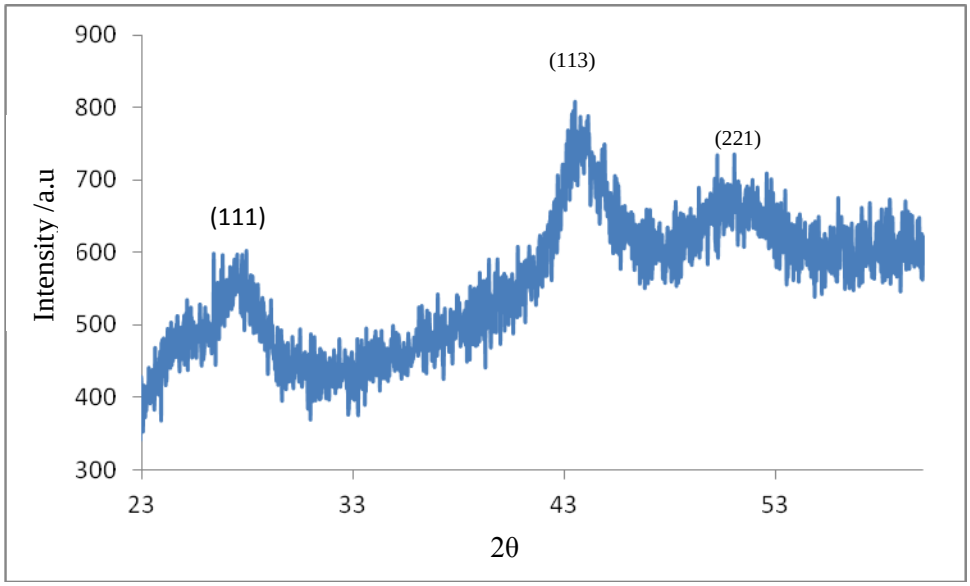

Figure 3.9. XRD spectrum of $LaEuF_3$-(Citric acid)-TTA nanoparticles.

3.3 $LaEuF_3$-(AEP)-HFA NANOPARTICLES (EUROPIUM-BASED DOWN-CONVERTING NANOPARTICLES: LOW TEMPERATURE METHOD)

We explored another fluorinated ligand as a surface coating ligand. A hexafluoro β-diketonate ligand, 1,1,1,5,5,5-hexatrifluoroacetylacetone (HFA) was tested as our sensitization ligand with the $LaEuF_3$ nanoparticle system.

3.3.1 UV-visible Absorption and Luminescence Studies

HFA-coated $LaEuF_3$-AEP nanoparticles showed an absorption peak at 305 nm. This peak is observed in the free HFA ligand confirming the HFA attachment (Figure 3.10A). The luminescence peak was observed at 614 nm. The observed luminescence was not bright compared to that observed for TTA coated nanoparticles. The quantum yields of $LaEuF_3$-(AEP)-HFA (16 mg) and $LaEuF_3$-(AEP)-HFA (32 mg) nanoparticles

are 0.29% and 0.78% respectvily. The relative quantum yield was lower for the $LaEuF_3$-(AEP)-HFA (32 mg) (0.78%) nanoparticles than that observed for $LaEuF_3$-(AEP)-TTA (32 mg) (4%) nanoparticles. The excited energy of the ligands (HFA and TTA) should match with the $^5D_0$ energy level of the Eu(III) ions. The triplet energy of the HFA ligand may not match with the $^5D_0$ energy level of the Eu(III) ions resulting a poor HFA ligand-to-metal energy transfer. This may be a reason for the observed low quantum yield of $LaEuF_3$-(AEP)-HFA nanoparticles.

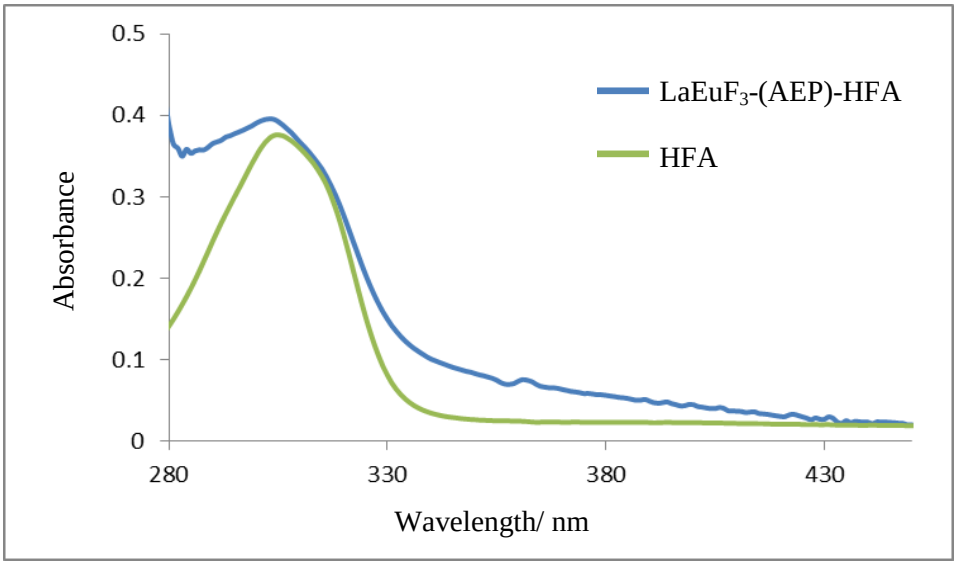

(A)

Figure 3.10. (A) UV-visible absorption spectrum of $LaEuF_3$-(AEP)-HFA (dispersed in a water / methanol solution)

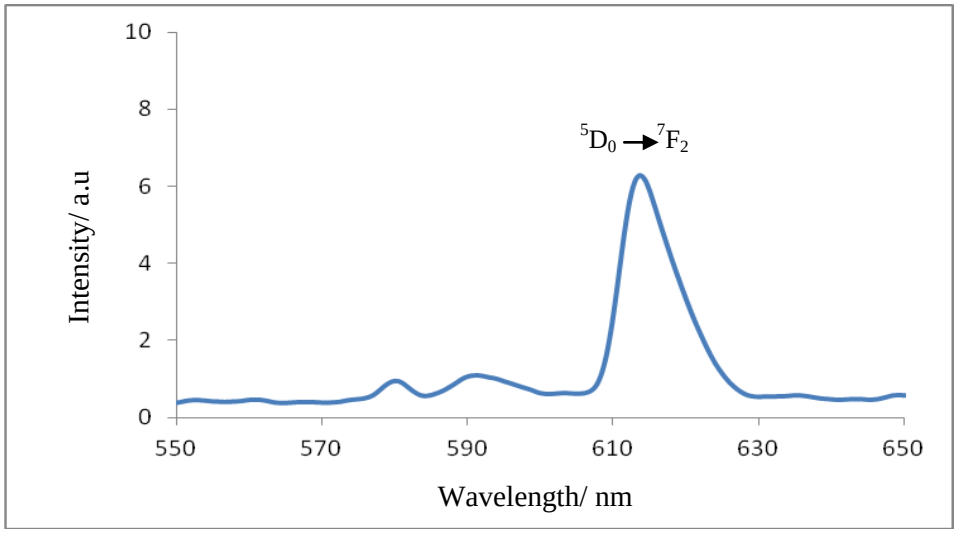

(B)

Figure 3.10. (B) Luminescence spectrum of $LaEuF_3$-(AEP)-HFA (excited at 305 nm).

3.3.2 X-Ray Powder Diffraction Studies

The XRD spectrum of $LaEuF_3$-(AEP)-HFA nanoparticles (Figure 3.11) confirms the hexagonal crystal structure observed for LaF_3 with peaks around 2θ positions of 27˚, 43˚, and 51˚.

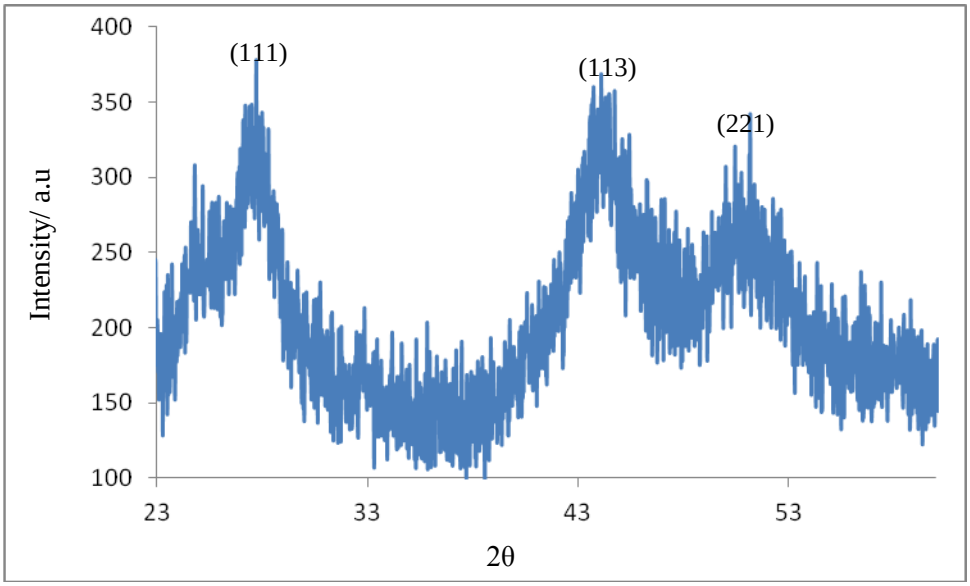

Figure 3.11. XRD spectrum of $LaEuF_3$-(AEP)-HFA nanoparticles.

3.4 $LaEuF_3$-MERCAPTOPROPIONIC ACID NANOPARTICLES (EUROPIUM-BASED DOWN-CONVERTING NANOPARTICLES: LOW TEMPERATURE METHOD)

Mercaptopropionic acid was used as another water soluble ligand instead of AEP. Use of mercaptopropionic acid as a surfactant was unsuccessful considering the poor water solubility of resulting nanoparticles. After the synthesis, a white colored, turbid solution was observed.

3.5 TTA COATED Eu:$NaYF_4$ NANOPARTICLES (HIGH TEMPERATURE METHOD)

$LaEuF_3$-AEP nanoparticles exhibit relatively low luminescence quantum yields with a large particle size. These particles, with an average diameter of 150 nm, may be used for *in-vitro* cell binding assays rather than *in-vivo* cell imaging. In order to prepare smaller nanoparticles, a high temperature method was utilized. Oleic acid coated Eu(III)-doped $NaYF_4$ nanoparticles were synthesized successfully using a high temperature decomposition method. This method involves dissolving lanthanide trifluoroacetate precursors in a high-boiling organic solvent (octadecane) with the assistance of a surfactant (oleic acid). Oleic acid is a very effective surfactant for producing small size nanoparticles.[28] The growth mechanism of nanocrystals has been systematically investigated, and it has been shown that the trifluoroacetate precursors in hot surfactant solutions go through a unique delayed nucleation pathway. This thermal decomposition method is effective and convenient for the preparation of the pure hexagonal (β) phase of $NaYF_4$ with morphologies and architectures including plates, spheres and ellipses controlled by varying the oleic acid surfactant concentration.[29,30] Even though this method was used to prepare small size nanoparticles, the hydrophobic nature of the oleic acid and the low luminescence efficiency are main drawbacks. We have developed a modified synthetic method to remove the hydrophobic oleic acid from the nanoparticle surface. This approach is based on an acid treatment protocol. At pH 4, oleic acid can be protonated and detached from the lanthanide nanoparticles. Oleic acid free nanoparticles were suspended in water and coated with the chromophore (TTA). Characterization of

oleic acid coated, oleic acid free and TTA coated Eu:$NaYF_4$ nanoparticles are discussed in this section.

3.5.1 Fourier Transform Infrared Studies

FT-IR spectra were obtained for solid nanoparticles as shown in Figure 3.12. The vibrational band in the FT-IR spectrum of oleic acid (Figure 3.12(A)) at 1703 cm^{-1} corresponds to the stretching vibration of the carbonyl group (C=O) in oleic acid. This vibrational band is absent in the oleic acid coated Eu:$NaYF_4$ nanoparticles (Figure 3.12(A)) and oleic acid free Eu:$NaYF_4$ nanoparticles (Figure 3.12(B)). Oleic acid molecules may be chemically adsorbed on the nanoparticle surface through coordination between the carboxylate group (COO^-) and the unsaturated lanthanide ions on the surface (Figure 3.13). The two peaks in the FT-IR spectrum of oleic acid coated Eu:$NaYF_4$ nanoparticles at 1564 cm^{-1} and 1465 cm^{-1} are due to the asymmetric and symmetric carboxylate group (COO^-) stretches, respectively. Oleic acid free nanoparticles maybe coated with surrounding water molecules. FT-IR spectrum of oleic acid free Eu:$NaYF_4$ nanoparticles shows peaks at 1653 cm^{-1} and 3358 cm^{-1} due to OH bending and stretching of water, respectively (Figure 3.12(B)). FT-IR spectrum of TTA coated Eu:$NaYF_4$ nanoparticles exhibits a characteristic peak around 1634 cm^{-1} due to the TTA attachment. The C=O stretching frequency in TTA coated Eu:$NaYF_4$ nanoparticles was shifted from 1640 cm^{-1} (Free TTA) (Figure 1.1(B) in Chapter 3, Section 3.1) to 1634 cm^{-1}.

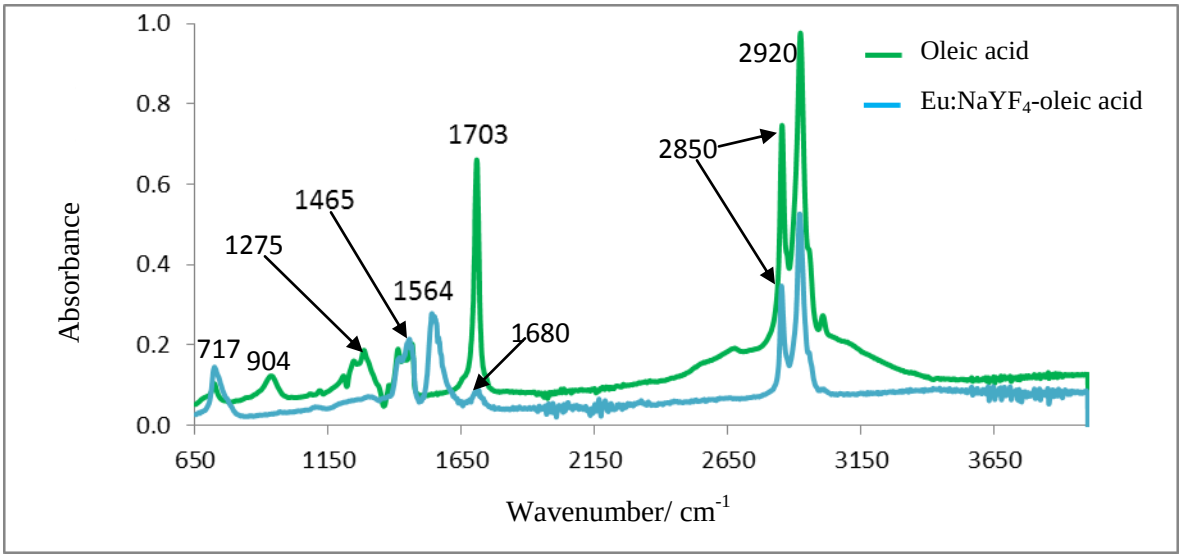

(A)

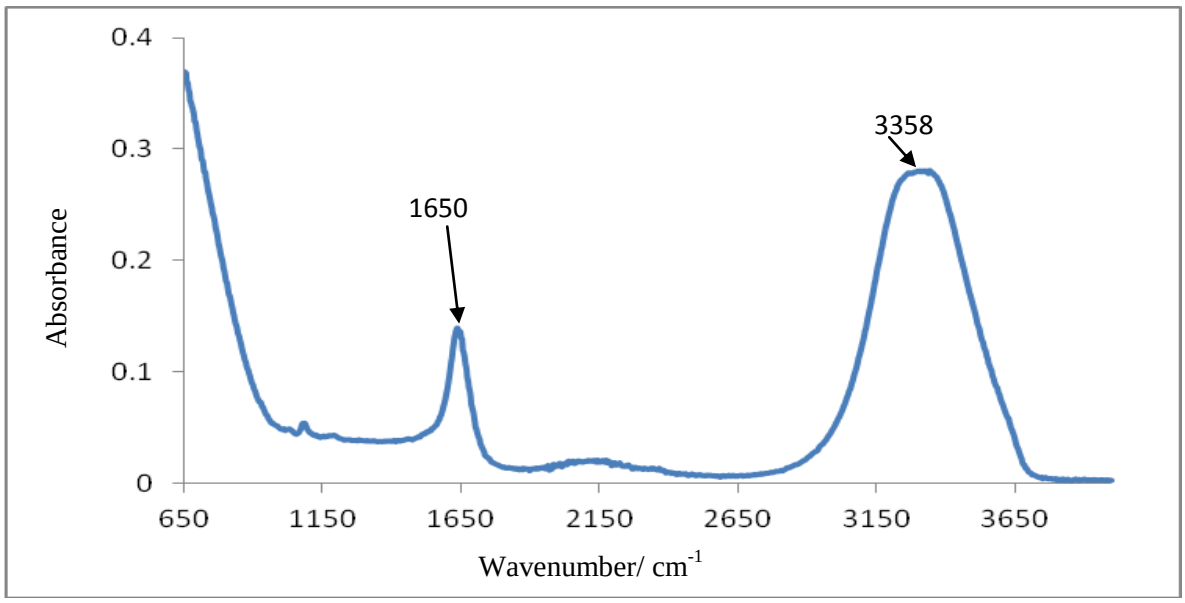

(B)

Figure 3.12. (A) FT-IR spectra of oleic acid and oleic acid coated Eu:$NaYF_4$ nanoparticles and (B) oleic acid free Eu:$NaYF_4$ nanoparticles.

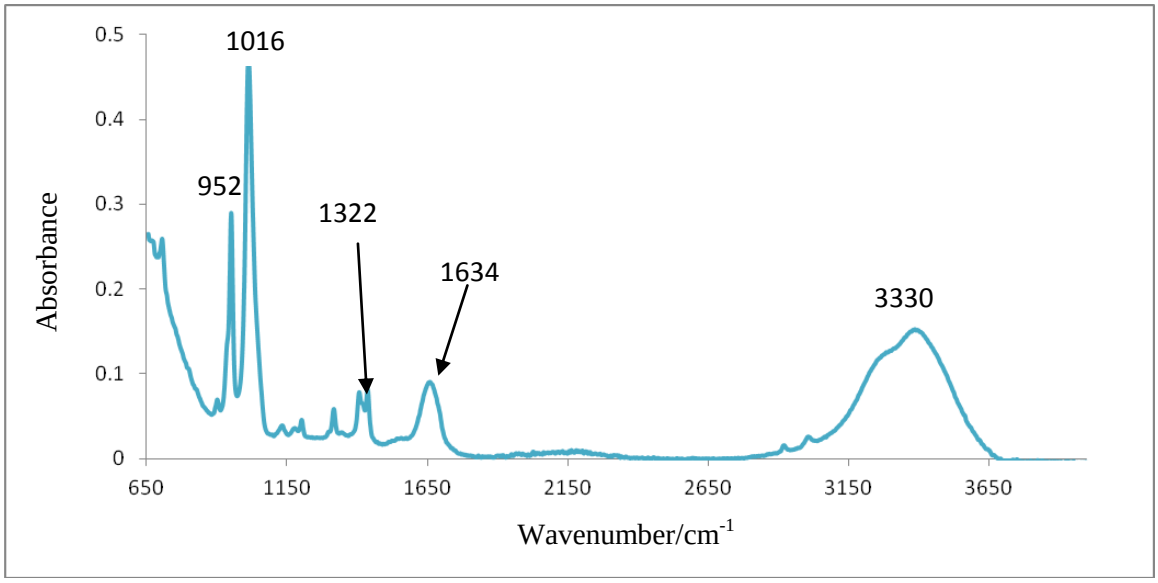

(C)

Figure 3.12. (C) FT-IR spectrum of TTA coated Eu:$NaYF_4$ nanoparticles.

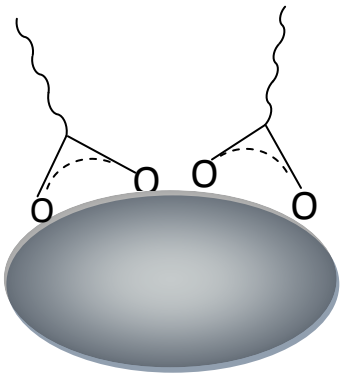

Figure 3.13. Schematic representation of the coordination of oleate in oleic acid coated Eu:$NaYF_4$ nanoparticles.

3.5.2 UV-visible Absorption and Luminescence Studies

Oleic acid coated Eu:$NaYF_4$ nanoparticles show a characteristic peak of oleic acid at 274 nm (Figure 3.14(A)). When oleic acid was removed from the nanoparticles, this characteristic peak was disappeared due to the absence of oleic acid. TTA coated Eu:$NaYF_4$ nanoparticles have a characteristic peak at 343 nm due to the TTA chromophore which was illustrated in Figure 3.2(A) (Chapter 3, Section 3.1).

Figure 3.14(B) illustrates the luminescence spectra of TTA coated Eu:$NaYF_4$ upon 343 nm excitation. The red fluorescence which is characteristic for Eu(III) (614 nm) was enhanced when 32 mg of TTA was used to coat the nanoparticles compared to when 16 mg of TTA was used. The quantum yields for TTA coated Eu:$NaYF_4$ nanoparticles are reported in Table 3.3. The highest quantum yield of 17 % was observed after using 32 mg of TTA ligand for the exchange process. This is a great enhancement in quantum yield when compared with $LaEuF_3$-(AEP)-TTA nanoparticles which have a quantum yield of 4% when an equivalent amount of TTA was used.

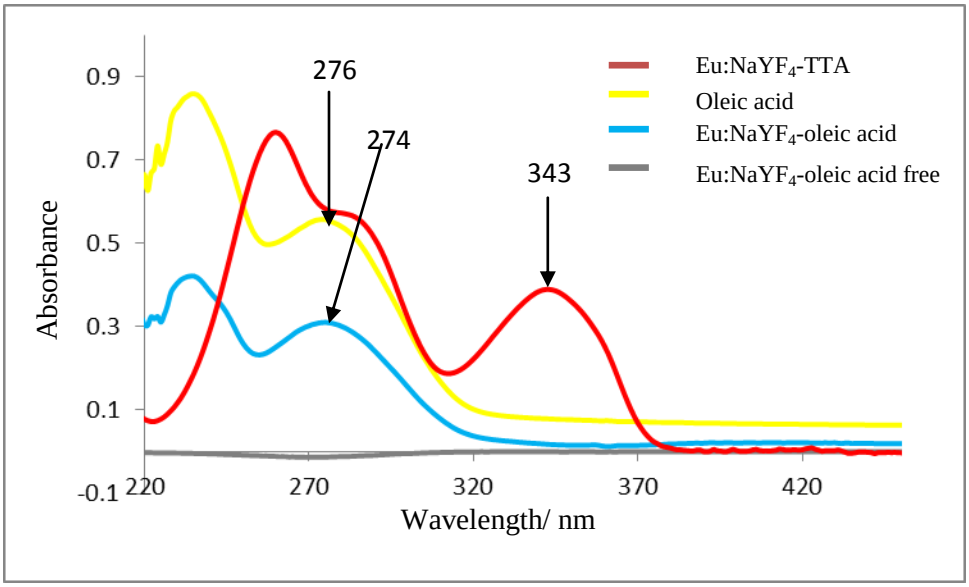

(A)

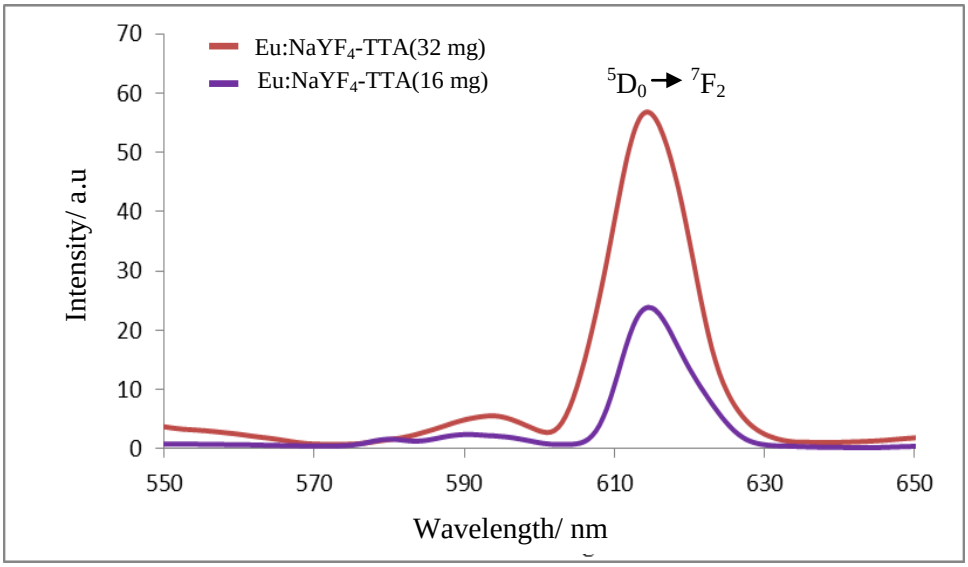

(B)

Figure 3.14. (A) UV-visible absorption spectra of oleic acid (dispersed in dichloromethane), oleic acid coated Eu:$NaYF_4$ (dispersed in dichloromethane), oleic acid free Eu:$NaYF_4$ (dispersed in water) and TTA coated Eu:$NaYF_4$ nanoparticles (dispersed in a methanol/water solution). (B) luminescence spectra of TTA coated Eu:$NaYF_4$ nanoparticles excited at 343 nm.

Table 3.3. Relative luminescence quantum yield values of the TTA coated Eu:$NaYF_4$ nanoparticles.

Nanoparticles	ϕ	Standard Deviation
Eu:$NaYF_4$-TTA (8 mg)	0%	0
Eu:$NaYF_4$-TTA (16 mg)	3.9%	0.892
Eu:$NaYF_4$-TTA (32 mg)	17.0%	1.023
Eu:$NaYF_4$-TTA (64 mg)	7.2%	0.978

3.5.3 X-Ray Powder Diffraction Studies

Oleic acid coated Eu:$NaYF_4$ nanoparticles exhibit a hexagonal crystal structure (Figure 3.15(A)). The peaks around 27˚, 32˚, 47˚ and 54˚ 2θ positions represent the (111), (200), (220) and (311) planes, respectively. Surface functionalization of Eu:$NaYF_4$ nanoparticles did not change the hexagonal crystal structure. After coating with TTA ligand, Eu:$NaYF_4$ nanoparticles show the same peaks in the XRD spectrum (Figure 3.15(C)). Oleic acid free Eu:$NaYF_4$ nanoparticles exhibited sharp peaks due to higher crystallinity (Figure 3.15(B)).

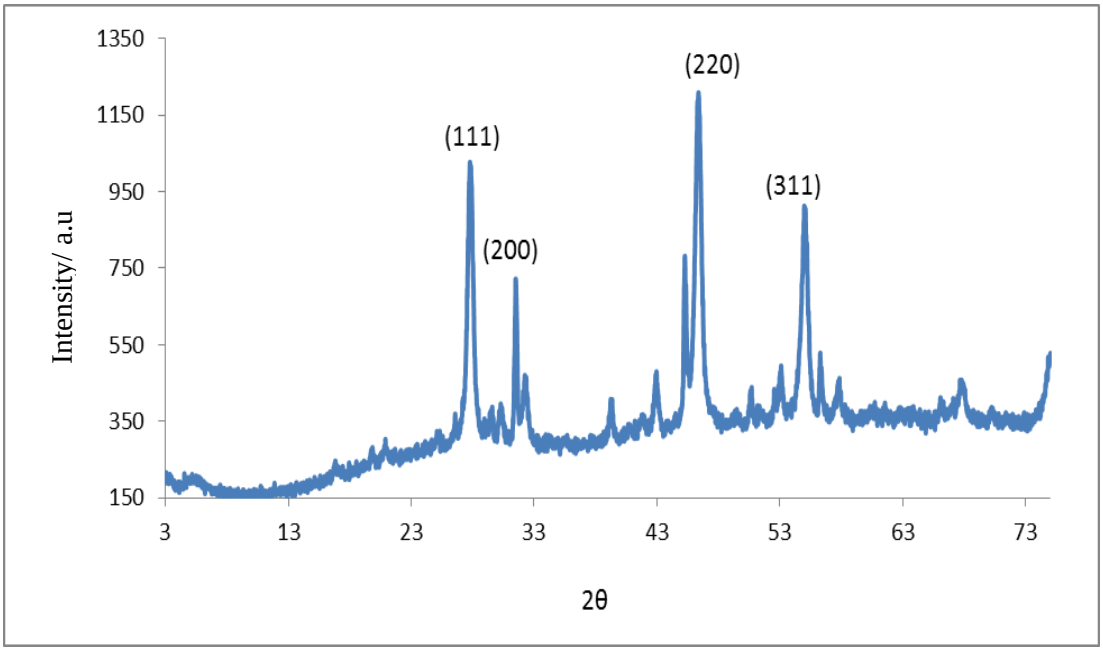

(A)

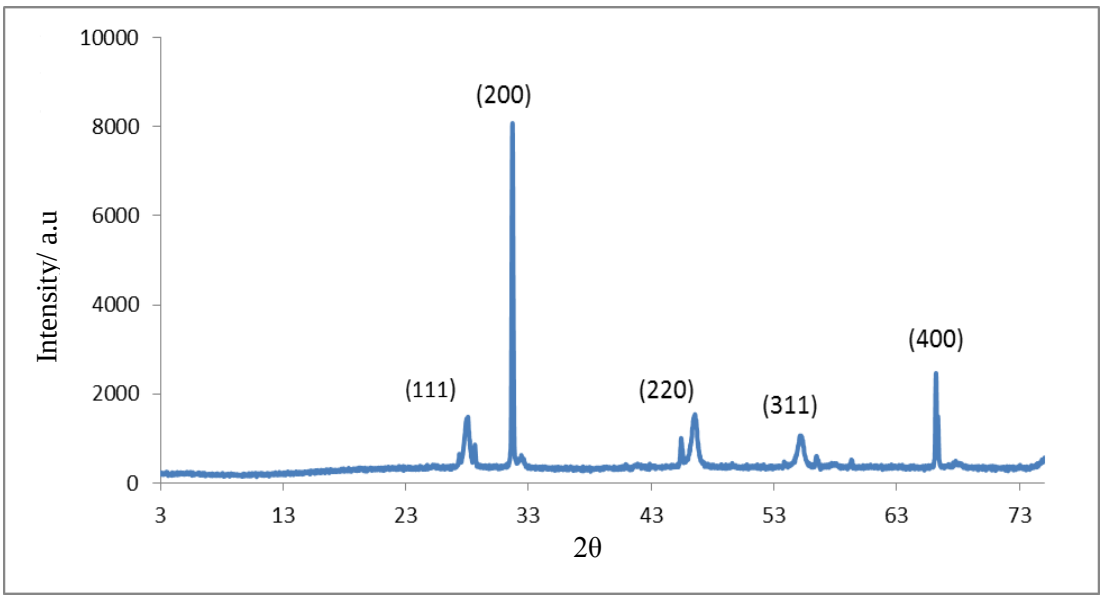

(B)

Figure 3.15. XRD spectra of (A) oleic acid coated Eu:$NaYF_4$ and (B) oleic acid free Eu:$NaYF_4$ nanoparticles.

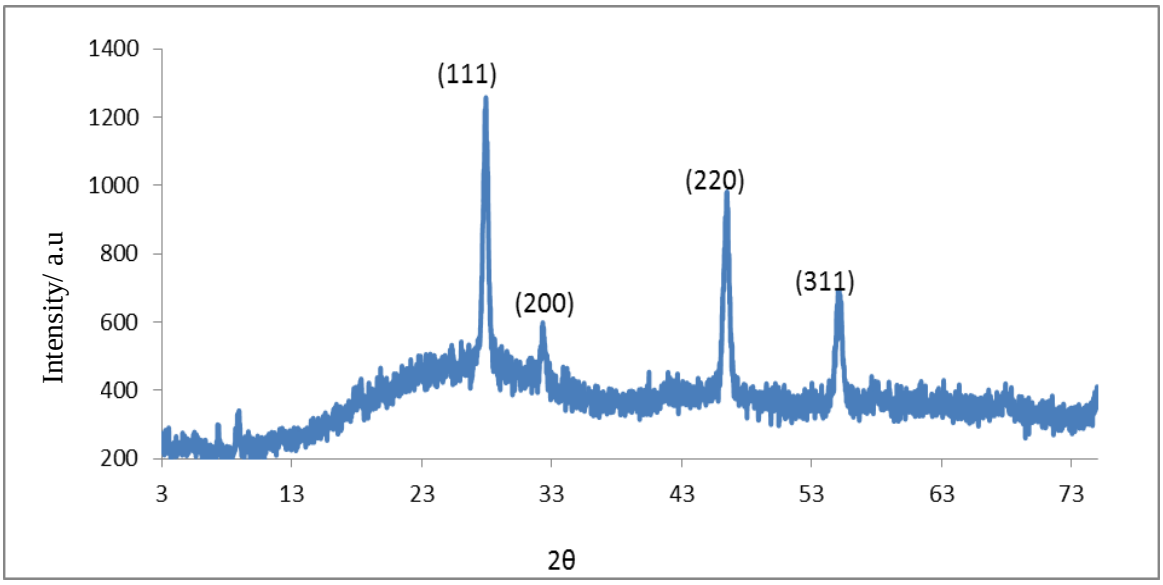

(C)

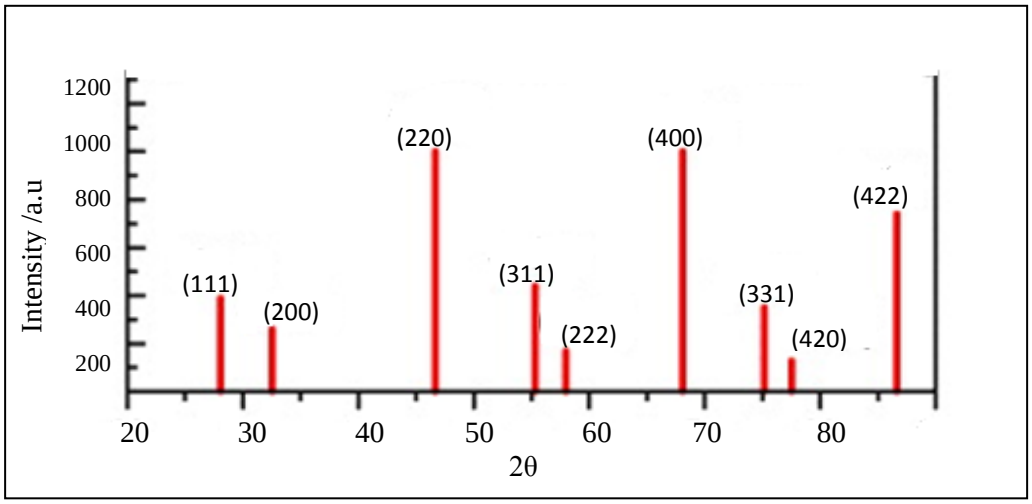

(D)

Figure 3.15. XRD spectra of (C) TTA coated Eu:$NaYF_4$ nanoparticles and (D) the reference spectrum for $NaYF_4$ hexagonal crystal structure (JCPDS NO. 27-0699).[31]

3.5.4 Luminescence Lifetime Studies

Luminescence lifetime measurements of Eu:$NaYF_4$ nanoparticles were carried out using 355 nm excitation wavelength. TTA coated Eu:$NaYF_4$ nanoparticles and oleic acid free Eu:$NaYF_4$ nanoparticles exhibit lifetimes of 1.8 ms and 1.7 ms, respectively (Figure 3.16). Eu:$NaYF_4$ nanoparticles exhibited higher lifetime than $LaEuF_3$ (650 µs and 900 µs) nanoparticles. This observation may be due to high crystallinity of the $NaYF_4$ nanoparticles than LaF_3 nanoparticles. High crystallinity favors low crystal defects resulting a longer luminescence lifetime with less luminescence quenching. Thus Eu:$NaYF_4$ nanoparticles have higher luminescence lifetime than that of $LaEuF_3$ nanoparticles. Lanthanide nanoparticles exhibit a longer lifetime than those observed for organic dyes. Rhodamine 6G and cy5 are some examples for organic dyes which are used for bio-medical imaging. Luminescence life times of Rhodamine 6G and cy5 are 4.08 ns and 1 ns, respectively.[32]

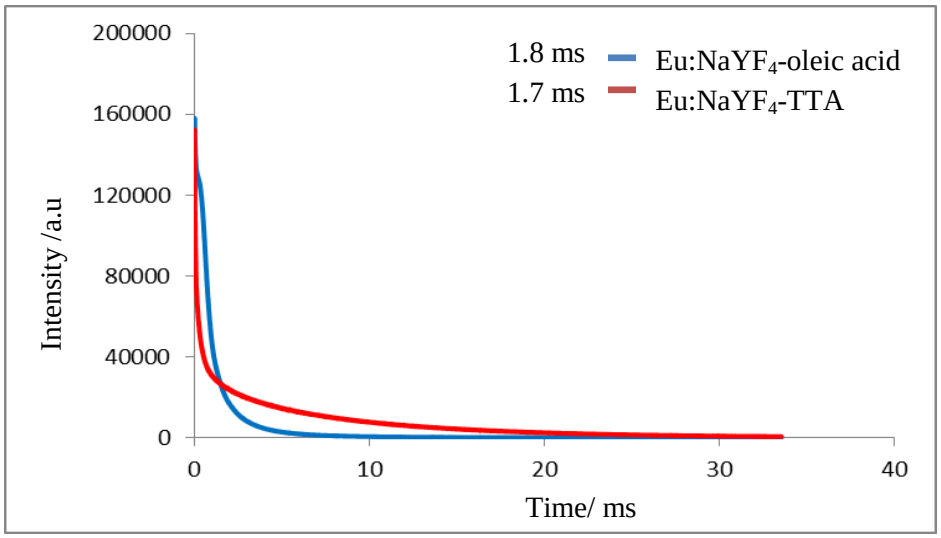

Figure 3.16. Luminescence lifetime measurements of Eu:$NaYF_4$ nanoparticles.

3.5.5 Transmission Electron Microscope (TEM) and Scanning Electron Microscope (SEM) Studies

According to TEM and SEM images, TTA coated Eu:$NaYF_4$ nanoparticles have an average particle diameter of 15 nm. This observed particle size is suitable for *in vitro and in vivo* cellular imaging which is an improvement when compared with $LaEuF_3$-(AEP)-TTA nanoparticles (150 nm) which were only suitable for *in vitro* studies. According to the modified Sheerer equation (Equation 4), the average diameter of the nanoparticles is 19 nm. Particle size distribution was calculated based on the TEM image as shown in Figure 3.18. Forty three percentages of the nanoparticles have a diameter of 21 nm.

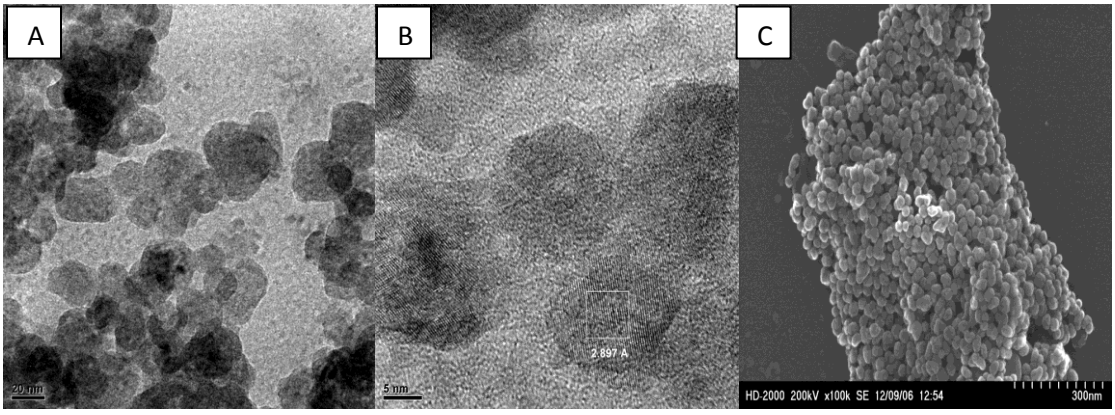

Figure 3.17. (A) TEM image (B) lattice structure (C) SEM image of Eu:$NaYF_4$-TTA nanoparticles.

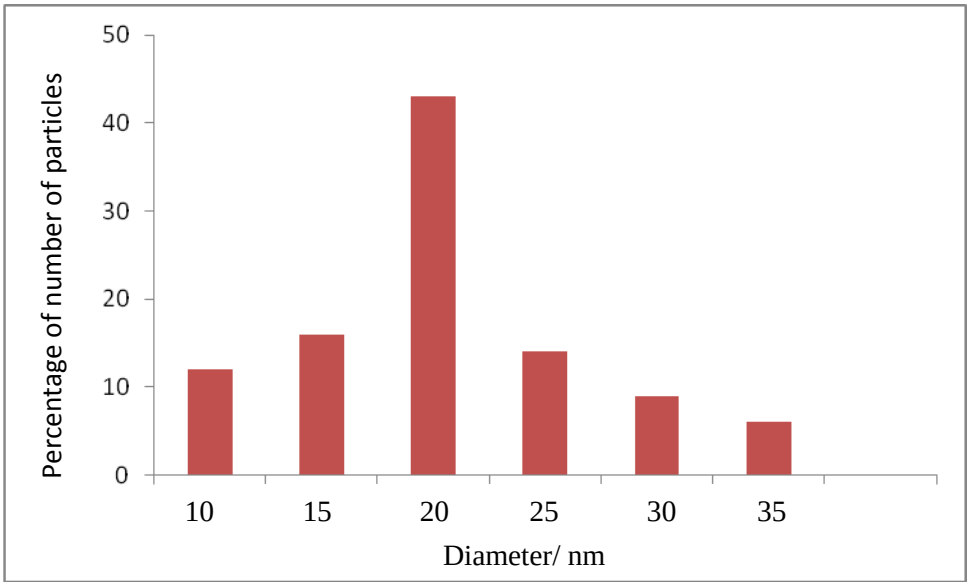

Figure 3.18. Particles size distribution of Eu:$NaYF_4$-TTA nanoparticles calculated from the TEM image.

3.5.6 Energy Dispersive X-Ray Mapping Studies (EDS)

EDS can be used to find the chemical composition of materials down to a spot size of a few microns, and to create elemental composition maps.[33] The EDS elemental map (Figure 3.19) endorses the elemental composition of oleic acid free Eu:$NaYF_4$ nanoparticles. Na, Y, Eu and F elements are present in Eu:$NaYF_4$-oleic acid free nanoparticles as shown in the EDS spectrum in Figure 3.20.

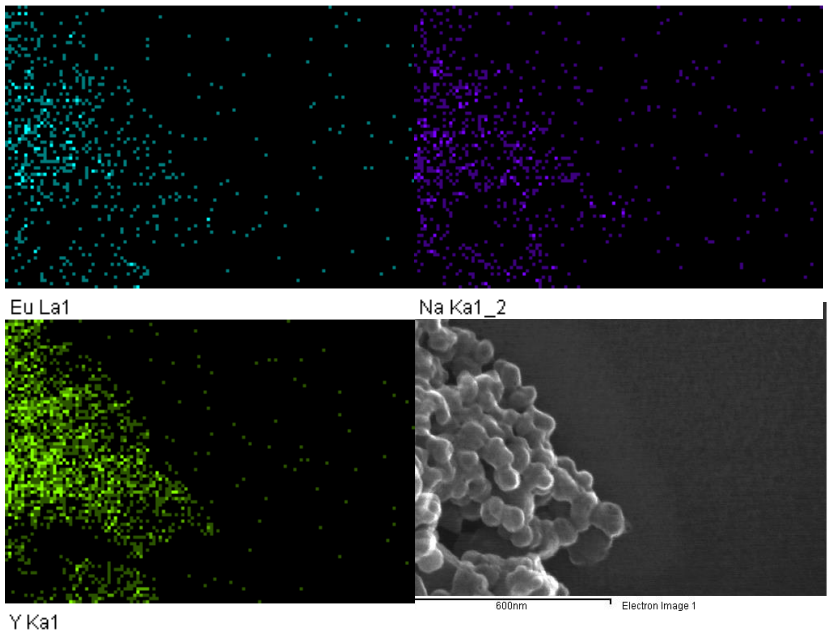

Figure 3.19. EDS elemental maps and SEM image of oleic acid free Eu:$NaYF_4$ nanoparticles (Y=green, Eu = blue, Na = purple).

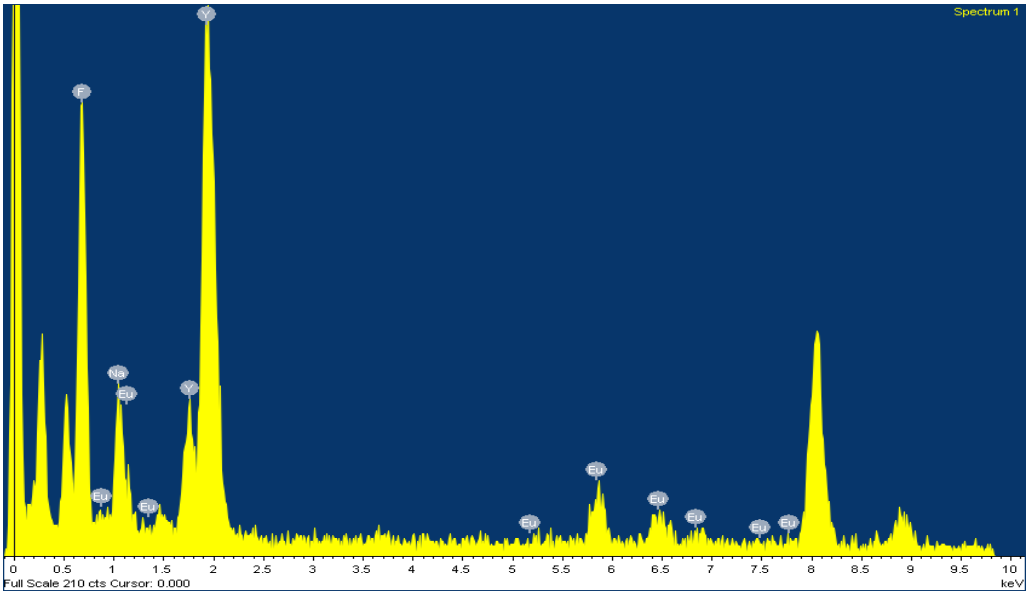

Figure 3.20. EDS spectrum of oleic acid free Eu:$NaYF_4$ nanoparticles.

3.5.7 Thermogravimetric Analysis (TGA)

The TGA diagram of oleic acid coated Eu:$NaYF_4$ nanoparticles shows mass losses around 147 ˚C, 292 ˚C and 398 ˚C (Figure 3.21(A)). The mass losses around 147 ˚C and 292 ˚C may be due to the removal of oleic acid. Those mass losses didn't appear in oleic acid free Eu:$NaYF_4$ nanoparticles due to the lack of oleic acid (Figure 3.21 (B)). The mass loss observed at 375 ˚C in oleic acid free Eu:$NaYF_4$ nanoparticles (Figure 3.21(B)) can be observed in the same temperature range in all Eu:$NaYF_4$ nanoparticles. This weight loss is the same for all three types of nanoparticle systems. We believe that this may be due to the decomposition of trifluoroacetate precursors that might have been adsorbed or trapped in the nanocrystals. Based on our mass assignments the mass percent of oleic acid in oleic acid coated Eu:$NaYF_4$ nanoparticles is 13.26%.

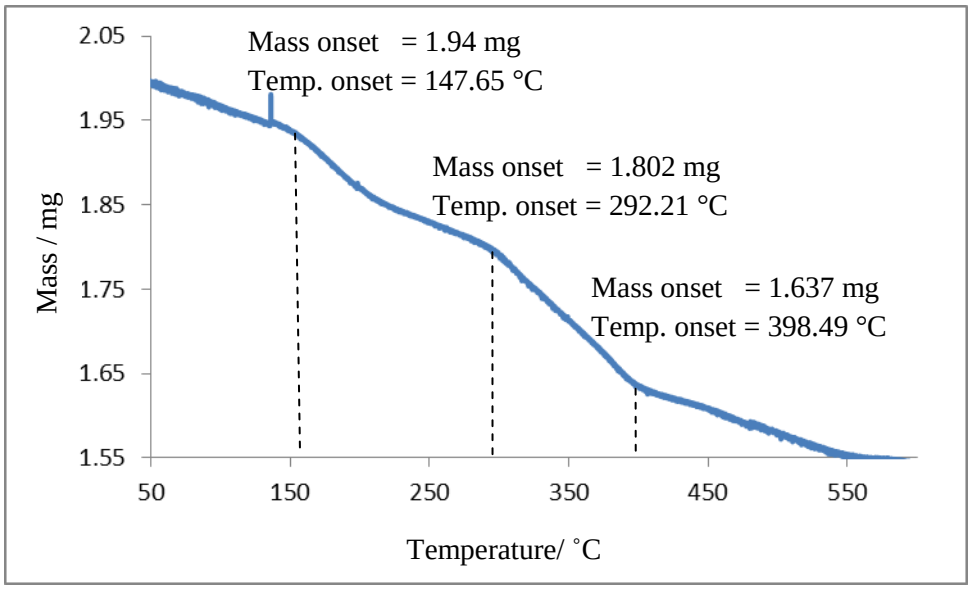

(A)

Figure 3.21. TGA diagram of (A) oleic acid coated Eu:$NaYF_4$ nanoparticles.

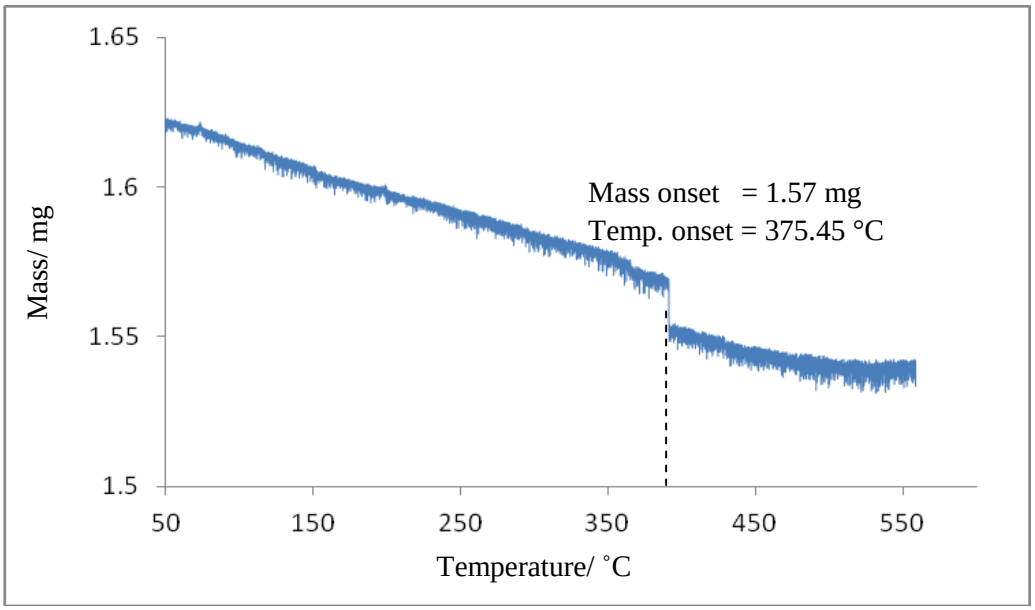

(B)

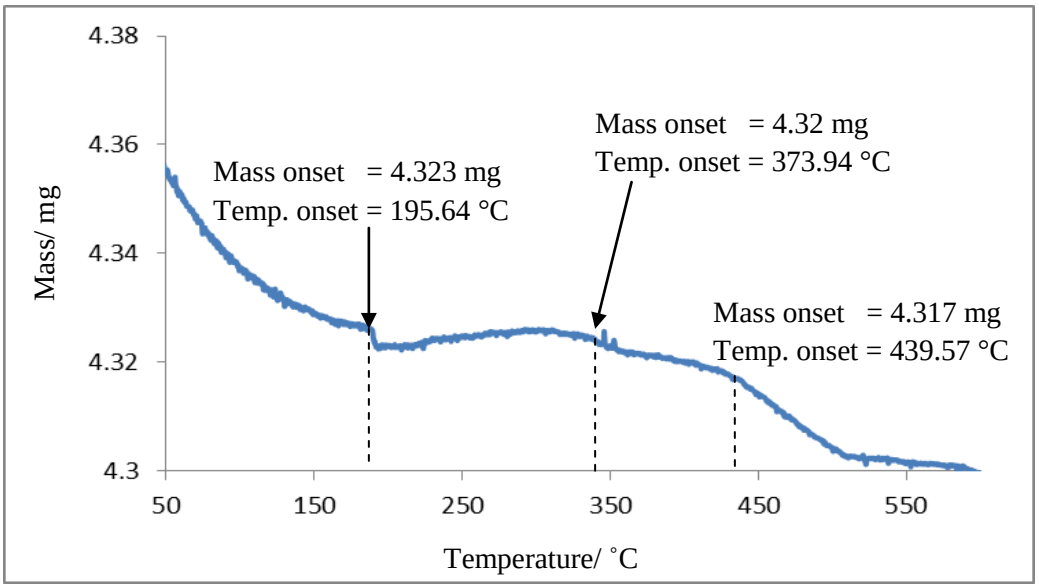

(C)

Figure 3.21. TGA diagrams of (B) oleic acid-free and (C) Eu:$NaYF_4$-TTA(8 mg) nanoparticles.

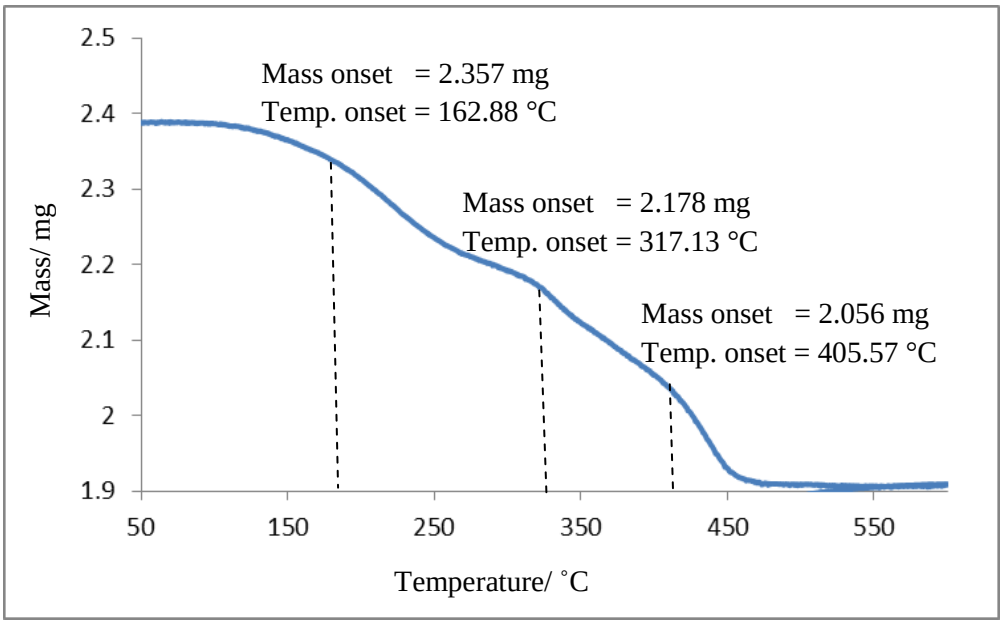

(D)

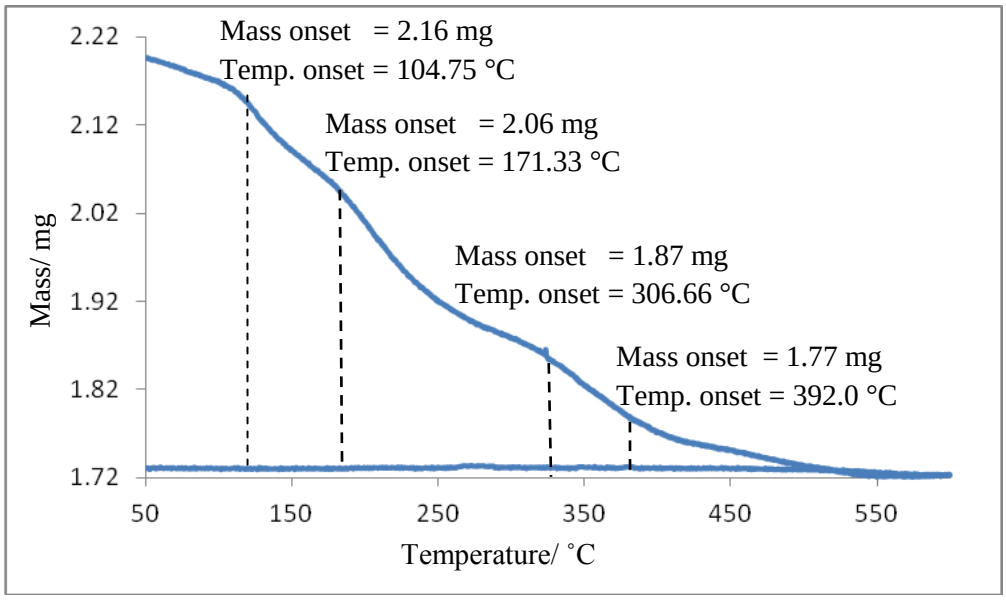

(E)

Figure 3.21. TGA diagrams of (D) Eu:$NaYF_4$-TTA(16 mg) and (E) Eu:$NaYF_4$-TTA (32 mg) nanoparticles.

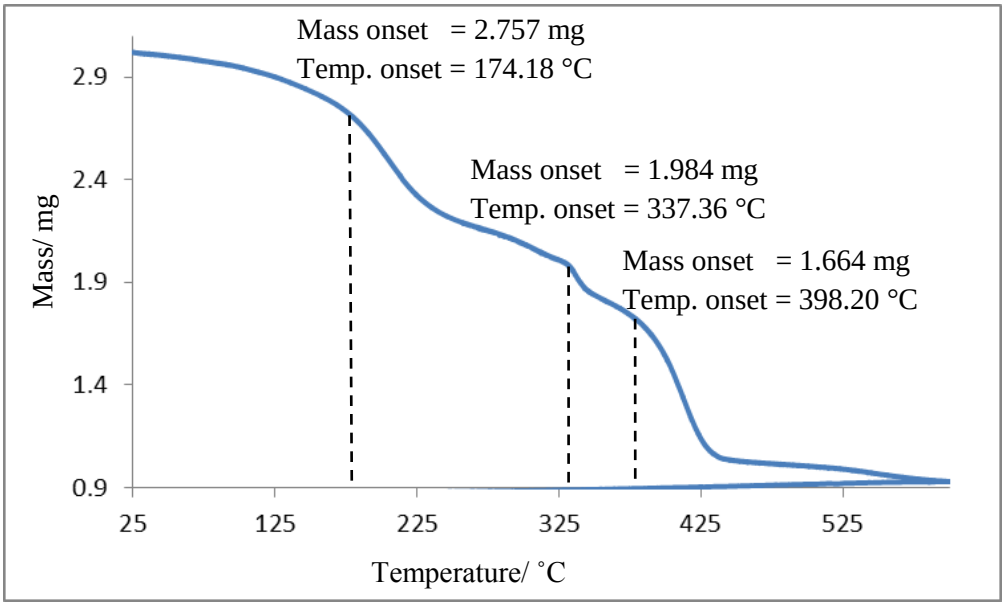

(F)

Figure 3.21. TGA diagrams of (F) Eu:$NaYF_4$-TTA(64 mg) nanoparticles.

The TGA diagram of 8 mg of TTA coated Eu:$NaYF_4$ nanoparticles did not exhibit clear weight losses (Figure 3.21(C)). The TTA mass percentage was 0.18%. This is low when compared with the TTA percentages observed for other nanoparticles (Table 3.4). Extremely low TTA percentage may be the reason that we were unable to measure the luminescence quantum yield of TTA(8mg)-coated Eu:$NaYF_4$ nanoparticles. The TGA diagram of 16 mg of TTA coated Eu:$NaYF_4$ nanoparticles shows weight losses at 162 ˚C, 317 ˚C and 405 ˚C (Figure 3.21(D)). TGA diagram of 32 mg of TTA coated Eu:$NaYF_4$ nanoparticles shows weight losses at 104 ˚C, 171 ˚C, 306 ˚C and 392 ˚C (Figure 3.21(E)). The weight loss around 104 ˚C may be due to the detachment of loosely bound water molecules. TGA diagram of 64 mg of TTA coated Eu:$NaYF_4$ nanoparticles also shows similar weight losses. We assume that the weight loss around 171 ˚C, 174 °C and 162 ˚C

may be due to the removal of TTA ligand. TTA percentages of nanoparticles were calculated using delta Y and step options (Table 3.4). The highest TTA mass percentage (12.53%) was observed for Eu:$NaYF_4$-TTA(32 mg) nanoparticles. Highest quantum yield was observed for the same nanoparticle system. This confirms that the highest TTA amount on the nanoparticle surface will give the highest quantum yield. When we compared with oleic acid mass percentage in oleic acid coated Eu:$NaYF_4$ nanoparticles, 13% may be the highest saturated surface coverage for Eu:$NaYF_4$ nanoparticle system.

Table 3.4. TTA mass percentages of Eu:$NaYF_4$-TTA nanoparticles (using the step option)

Nanoparticles	Mass percentage of TTA (%)
Eu:$NaYF_4$-TTA (16 mg)	0.18
Eu:$NaYF_4$-TTA (16 mg)	7.69
Eu:$NaYF_4$-TTA (32 mg)	12.53
Eu:$NaYF_4$-TTA (64 mg)	9.73

3.6 btfa COATED Eu:$NaYF_4$ NANOPARTICLES (HIGH TEMPERATURE METHOD)

Oleic acid free Eu:$NaYF_4$ nanoparticles were surface functionalized with another β-diketone (chromophore), namely 4,4,4-trifluoro-1-pheny-1,3-butanedione (btfa). 32 mg and 16 mg of btfa ligand were used for the surface functionalization of oleic acid free Eu:$NaYF_4$ nanoparticles (75 mg) using a similar ligand exchange process used for TTA coating (Chapter, Section 2.2.2). The quantum yield was calculated for btfa coated Eu:$NaYF_4$ nano- particles using cresyl violet acetate as the standard. Observed quantum yield values were 4.2% and 4.0% for 32mg and 16 mg of btfa coated Eu:$NaYF_4$ nanoparticles, respectively. When compared with TTA ligand, we confirm that btfa was not an efficient sensitizer ligand for the Eu:$NaYF_4$ nanoparticles.

3.6.1 UV-visible Absorption and Luminescence Studies

UV-visible absorption spectrum of the btfa ligand (Figure 3.22(A)) exhibited a peak at 324 nm. btfa coated Eu:$NaYF_4$ nanoparticles have the same characteristic peak at 324 nm confirming the presence of the btfa ligand in Eu:$NaYF_4$ nanoparticles. The luminescence spectrum upon 324 nm excitation (Figure 3.22(B)) displayed a peak at 614 nm which is unique to Eu(III) ions.

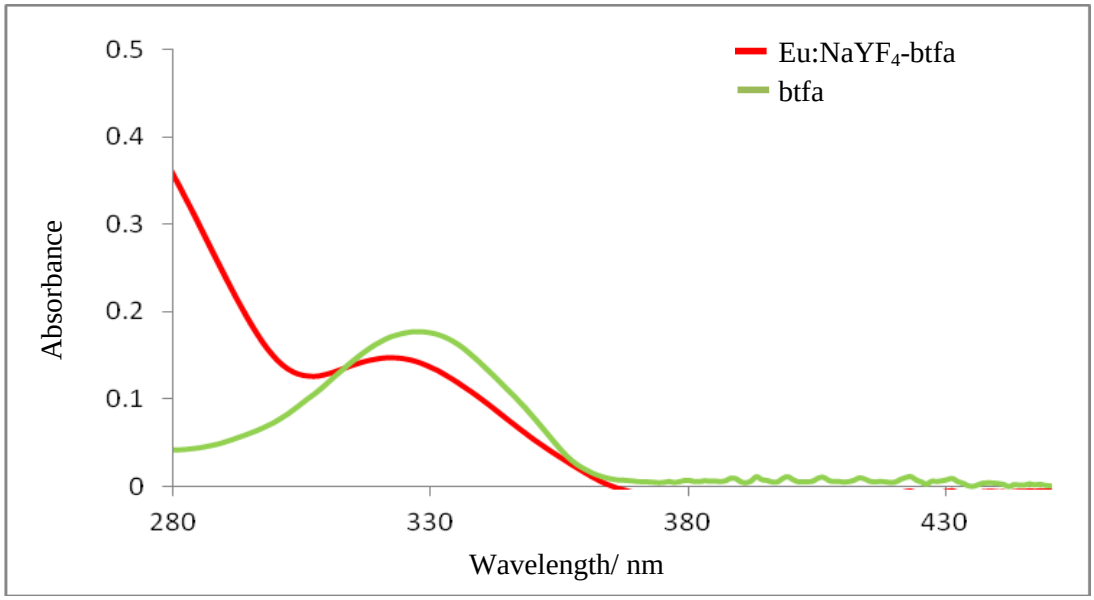

(A)

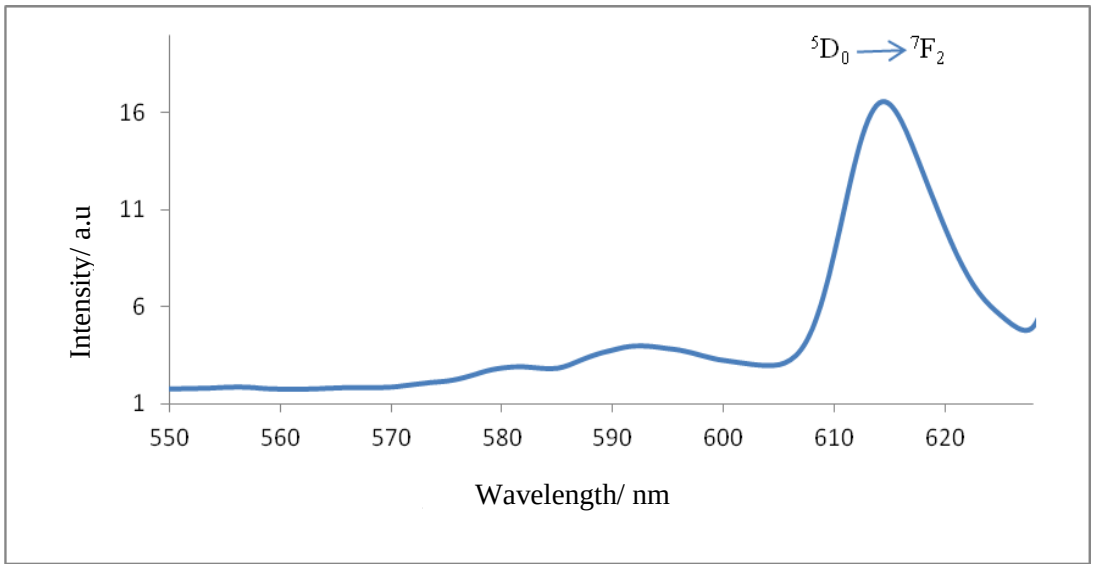

(B)

Figure 3.22. (A) UV-visible absorption spectrum and (B) luminescence studies of btfa coated Eu:$NaYF_4$ nanoparticles (dispersed in a water/ methanol solution).

3.7 TTA COATED Eu:$NaYF_4$-MSH4 NANOPARTICLES (HIGH TEMPERATURE METHOD)

The ultimate goal of this project is to attach the MSH4 (melanocyte stimulating hormone) peptide ligand to the nanoparticle surface for potential imaging of melanoma cancer cells. Oleic acid free Eu:$NaYF_4$ nanoparticles were surface functionalized with MSH4 hormone, and afterward these nanoparticles were coated with TTA ligand.

3.7.1 Fourier Transform Infrared Studies

FT-IR spectra were collected for solid particles of MSH4 and Eu:$NaYF_4$-MSH4 nanoparticles as shown in Figure 3.23. The IR spectrum of Eu:$NaYF_4$-MSH4 nanoparticles exhibited some characteristic peaks due to MSH4 hormone as shown in Figure 3.23(A) and (B). The peaks at 1653 cm^{-1}, 2990 cm^{-1} and 3338 cm^{-1} were common for both IR spectra of MSH4 and Eu:$NaYF_4$-MSH4 although the latter two are red shifted by 45 cm^{-1} and 10 cm^{-1} respectively in the nanoparticles spectrum. The IR spectrum of TTA coated Eu:$NaYF_4$-MSH4 (Figure 3.23(C)) exhibits the peak around 1643 cm^{-1} due to TTA attachment (IR spectrum of free TTA shown in the Chapter 3, Section 3.1, Figure 3.1) .

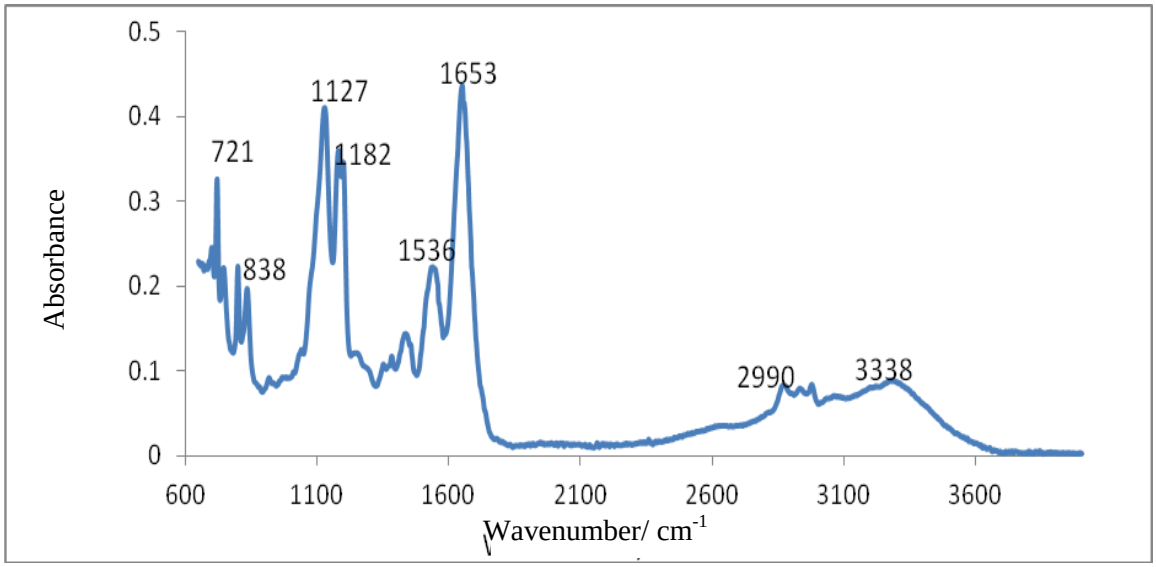

(A)

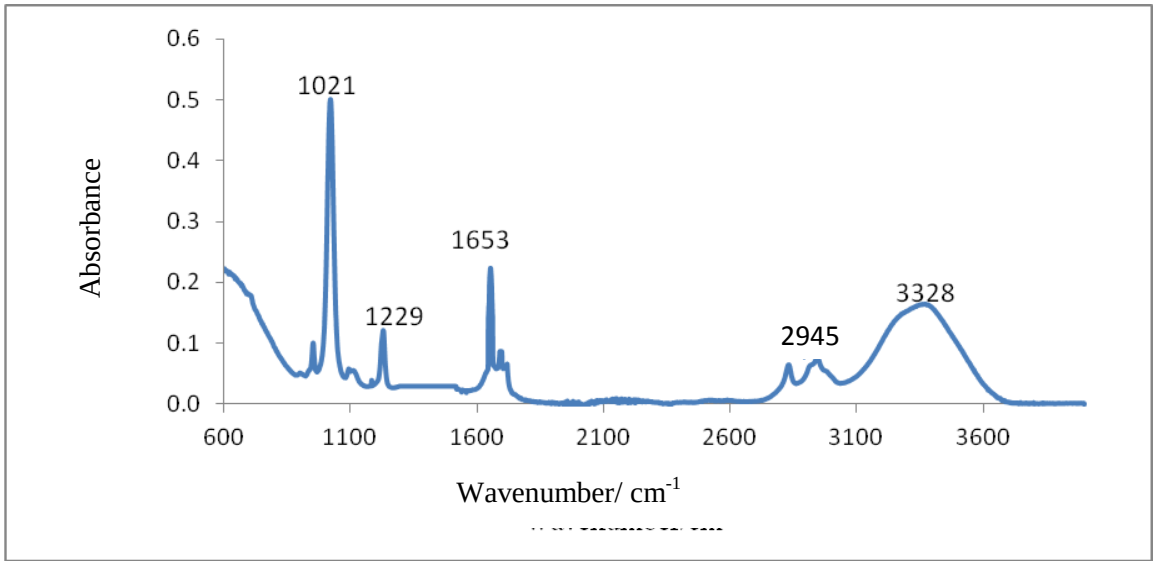

(B)

Figure 3.23. FT-IR spectra of (A) MSH4 peptide and (B) Eu:$NaYF_4$-MSH4 nanoparticles.

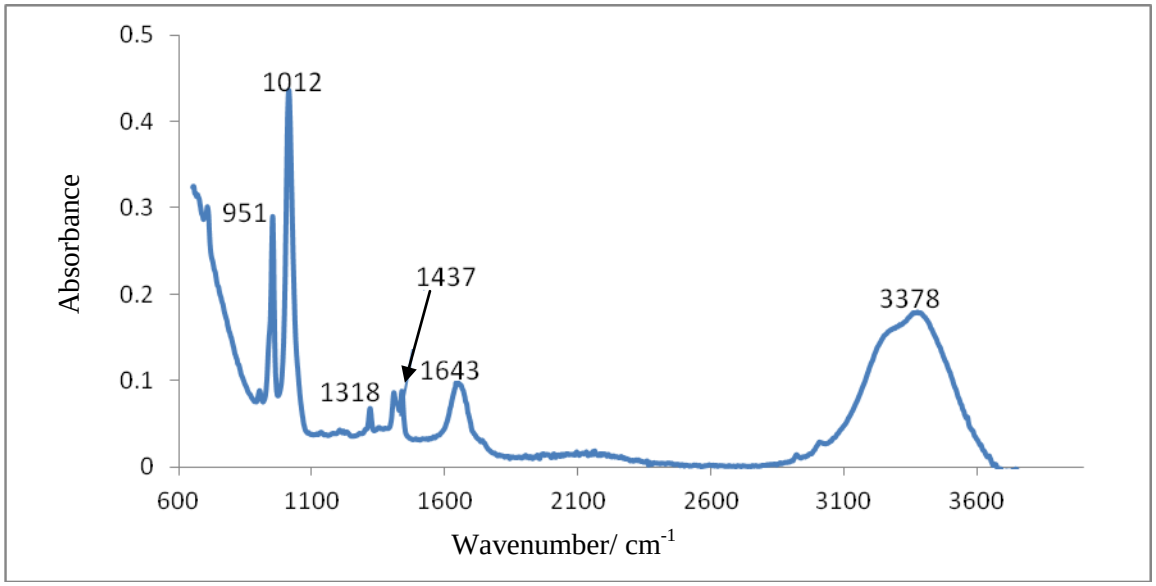

(C)

Figure 3.23. FT-IR spectrum of (C) TTA coated Eu:$NaYF_4$-MSH4 nanoparticles.

3.7.2 UV-visible Absorption and Luminescence Studies

MSH4 peptide shows a characteristic absorption peak at 290 nm as shown in Figure 3.24 (A). The UV-visible spectrum of TTA coated Eu:$NaYF_4$-MSH4 nanoparticles (Figure 3.24(A)) presented this characteristic absorption band due to the presence of MSH4 peptide. In addition, TTA coated Eu:$NaYF_4$-MSH4 exhibits a peak at 343 nm confirming the presence of TTA ligand (UV- visible spectrum of free TTA is shown in the Chapter 3, Section 3.1, Figure 3.2). According to the luminescence spectrum (Figure 3.24(A)), the Eu(III) peak can be recognized at 614 nm upon 343 nm excitation. The quantum yield for the TTA coated Eu:$NaYF_4$-MSH4 nanoparticles is

calculated to be 0.4%. This value has to be optimized by using different ligand combinations of MSH4/TTA. This will be a scope of a future project.

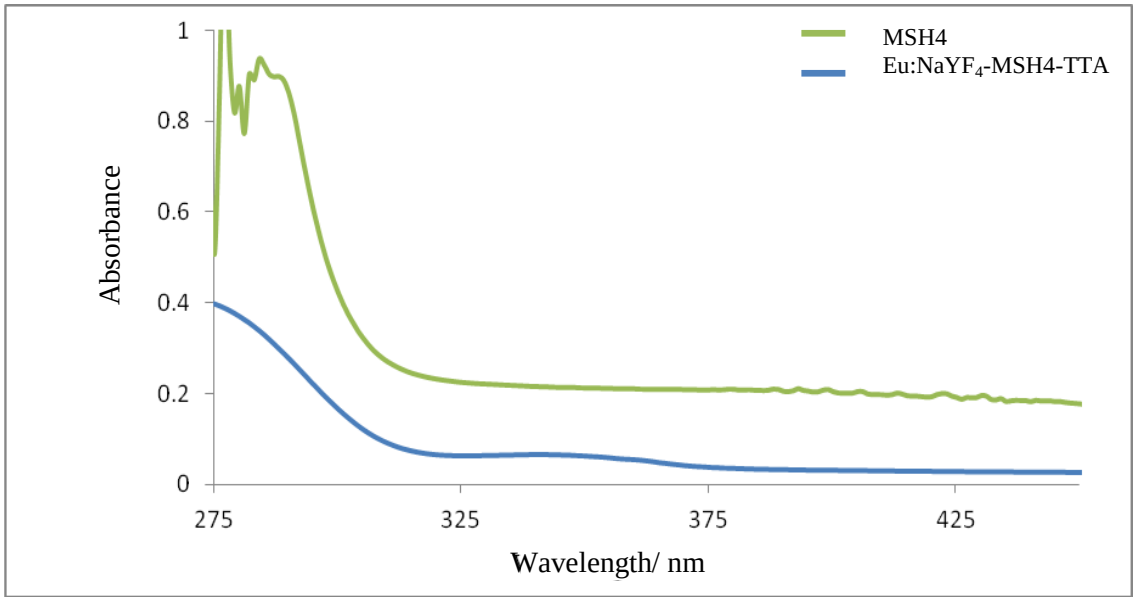

(A)

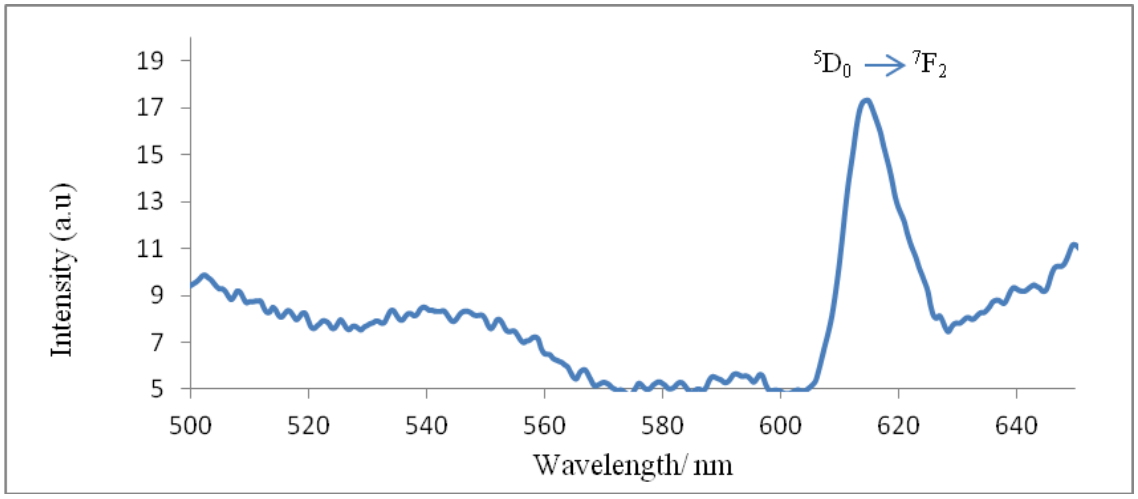

(B)

Figure 3.24. (A) UV-visible absorption spectrum and (B) luminescence spectrum of TTA coated Eu:$NaYF_4$-MSH4 nanoparticles (dispersed in a methanol/ water solution).

3.7.3 X-Ray Powder Diffraction Studies

The XRD spectrum of TTA coated Eu:$NaYF_4$-MSH4 nanoparticles inveterates the identical hexaganal crystal structure of Eu:$NaYF_4$ nanoparticles as shown in Figure 3.25. All the diffraction positions agreed with the hexaganal structure of $NaYF_4$ crystals.

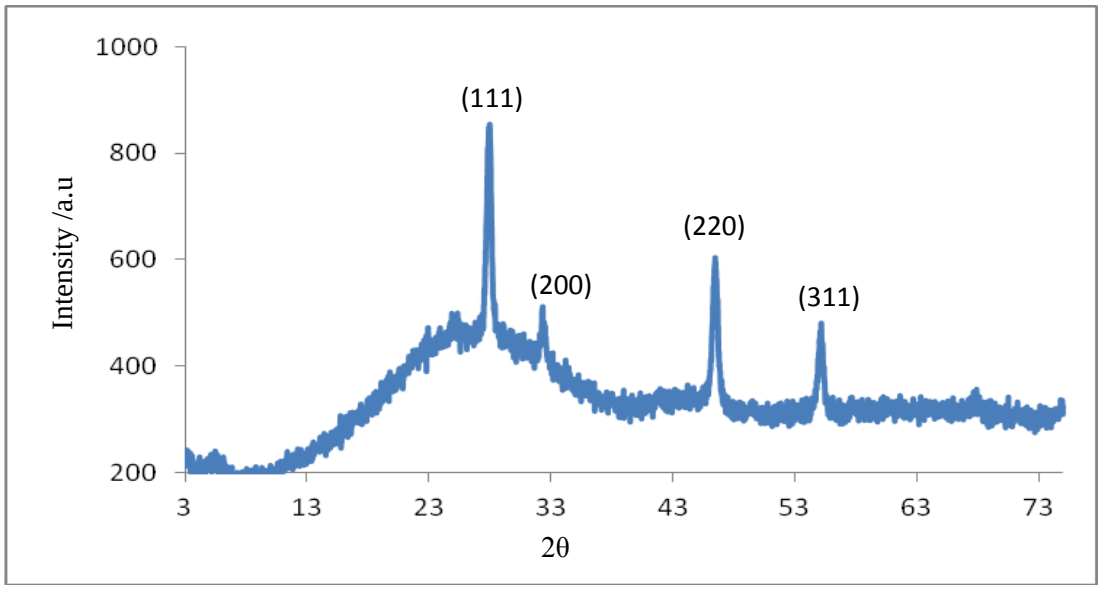

Figure 3.25. XRD spectrum of TTA coated Eu:$NaYF_4$-MSH4 nanoparticles.

3.7.4 Transmission Electron Microscope (TEM) and Scanning Electron Microscope Studies (SEM)

TEM and SEM images of TTA coated Eu:$NaYF_4$-MSH4 nanoparticles are depicted in Figure 3.26. The morphology of the nanoparticles is roughly spherical with an average particle diameter of 18 nm promising for biomedical imaging applications.

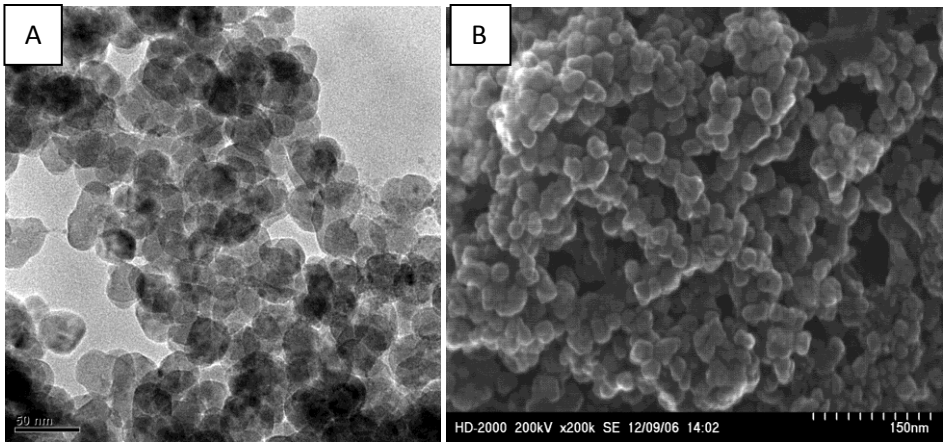

Figure 3.26. (A) TEM image and (B) SEM image of TTA coated Eu:$NaYF_4$-MSH4 nanoparticles.

3.8 UPCONVERTING NANOPARTICLES

Upconverting nanoparticles have drawn recent interest in their use in biological systems due to harmless infrared excitation with minimum background fluorescence. Upconverting nanoparticles (Yb:Er:$NaYF_4$) were synthesized by using oleic acid as the surfactant. Oleic acid was removed from the nanoparticle surface as was done in Eu:$NaYF_4$ nanoparticle synthesis. Oleic acid free Yb:Er:$NaYF_4$ nanoparticles were freely dispersible in water. Bare Yb:Er:$NaYF_4$ nanoparticles were coated with aminoethyl phosphate (AEP) to improve the water dispersibility and future surface functionality. AEP is an efficient linker for attaching the MSH4 peptide ligand. Due to amino carboxylate coupling, AEP coated nanoparticles can efficiently be attached to MSH4 peptide using peptide coupling.

3.8.1 Fourier Transform Infrared Studies

IR spectrum of oleic acid coated Yb:Er:$NaYF_4$ revealed identical peak positions corresponding to the oleic acid coated Eu:$NaYF_4$ nanoparticles. The peaks around 1537 cm^{-1} and 1444 cm^{-1} confirmed the COO^- attachment of nanoparticles (Figure 3.27(A)). The peaks corresponding to oleic acid were diminished in the IR spectrum of oleic acid free Yb:Er:$NaYF_4$ nanoparticles (Figure 3.27(B)). The same peak observed for Eu:$NaYF_4$ nanoparticles around 1653 cm^{-1} was observed in the IR spectra of oleic acid free Yb:Er:$NaYF_4$ nanoparticles.

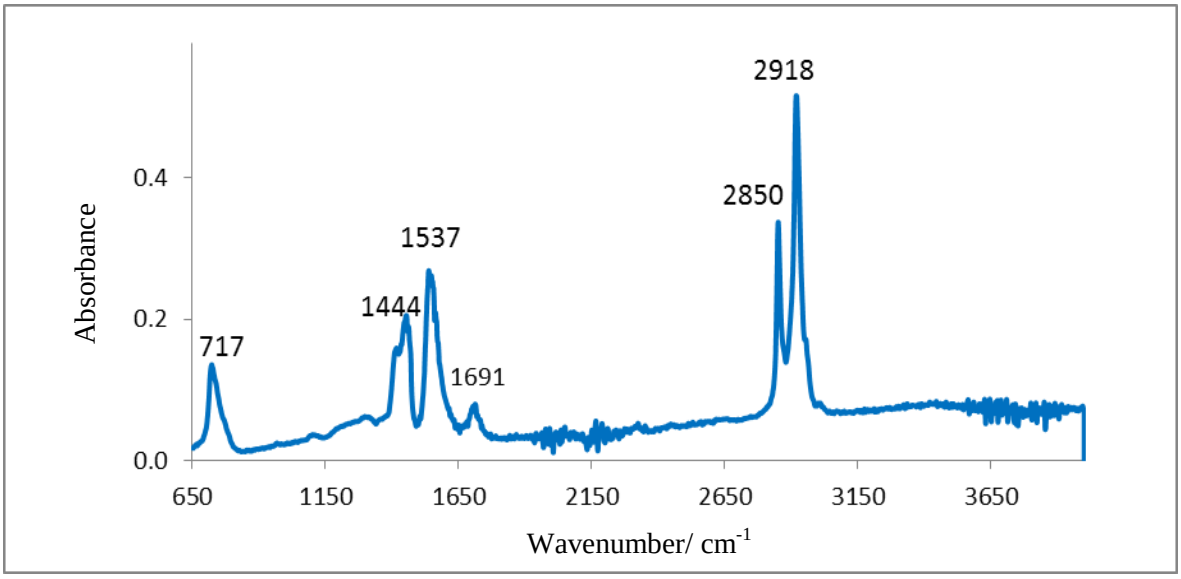

(A)

Figure 3.27. IR spectrum of (A) oleic acid coated Yb:Er:$NaYF_4$ nanoparticles.

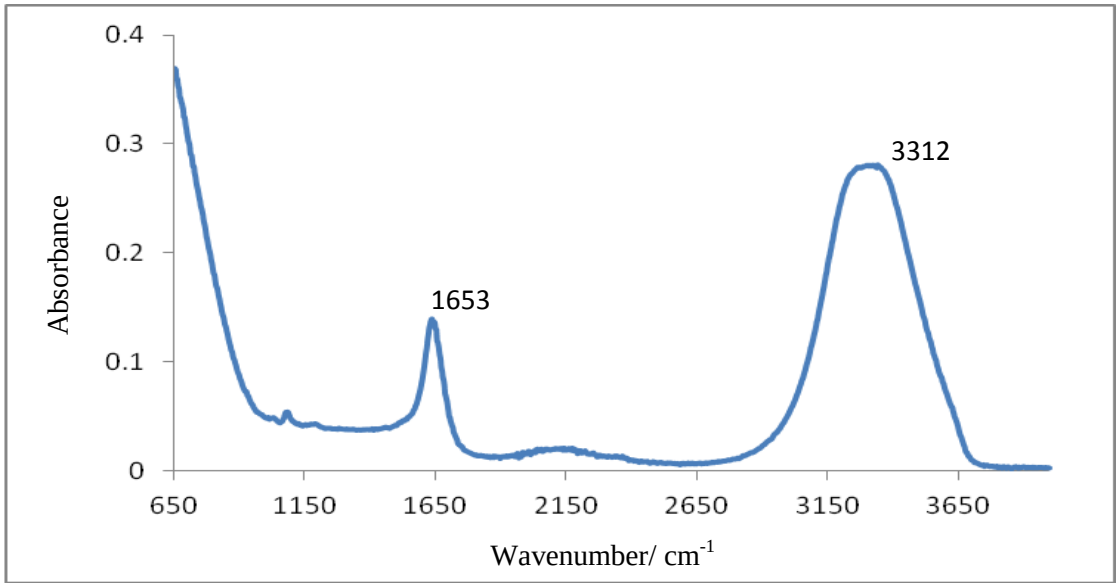

(B)

Figure 3.27. IR spectrum of (B) oleic acid free Yb:Er:$NaYF_4$ nanoparticles.

3.8.2 X-Ray Powder Diffraction Studies

XRD patterns of the Yb:Er:$NaYF_4$ nanoparticles (Figure 3.28) exhibit peak positions and intensities that can be well indexed in accordance with the hexagonal structure of $NaYF_4$ crystals suggesting high crystallinity of the product. The dopant metal ions and levels did not change the parental crystal structure of the material.

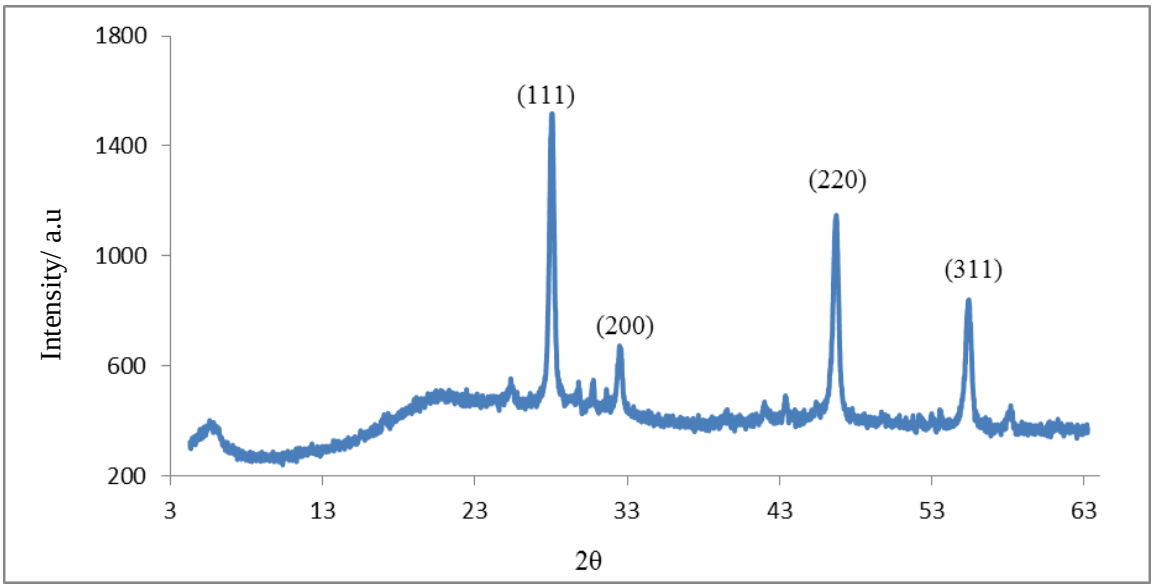

(A)

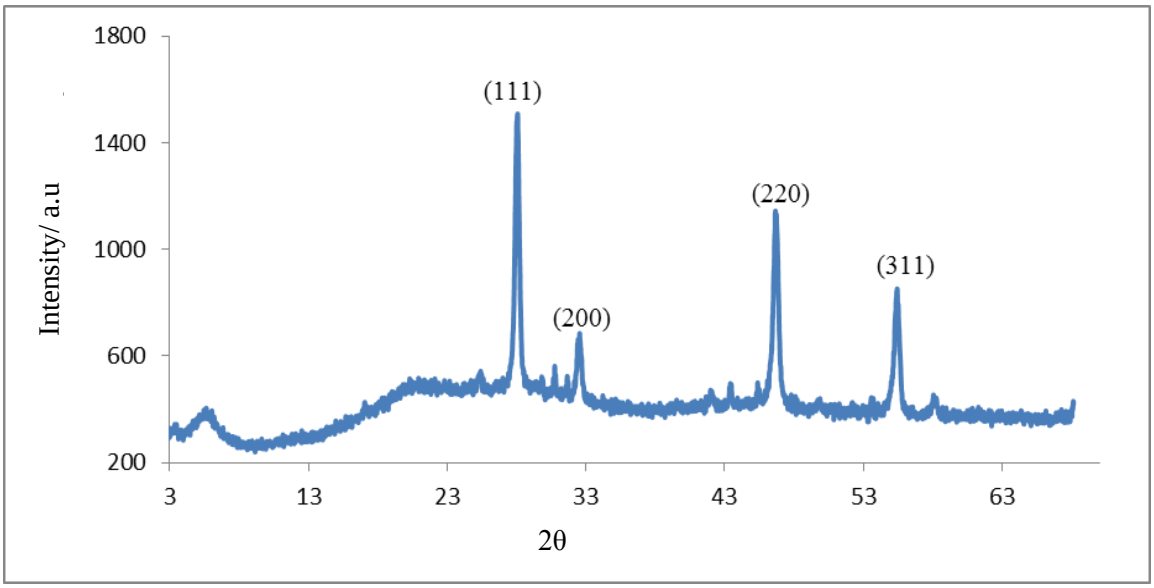

(B)

Figure 3.28. XRD spectra of (A) oleic acid coated Yb:Er:$NaYF_4$ nanoparticles and (B) AEP coated Yb:Er:$NaYF_4$ nanoparticles.

3.8.3 Transmission Electron Microscope (TEM) and Scanning Electron Microscope Studies (SEM)

The high resolution TEM image shows spherical morphology of the Yb:Er:$NaYF_4$-AEP nanoparticles with an average particle diameter of 19 nm. According to the TEM image, particle diameter distribution was presented in Figure 3.30. Forty six percent of the nanoparticles have a diameter of 20 nm.

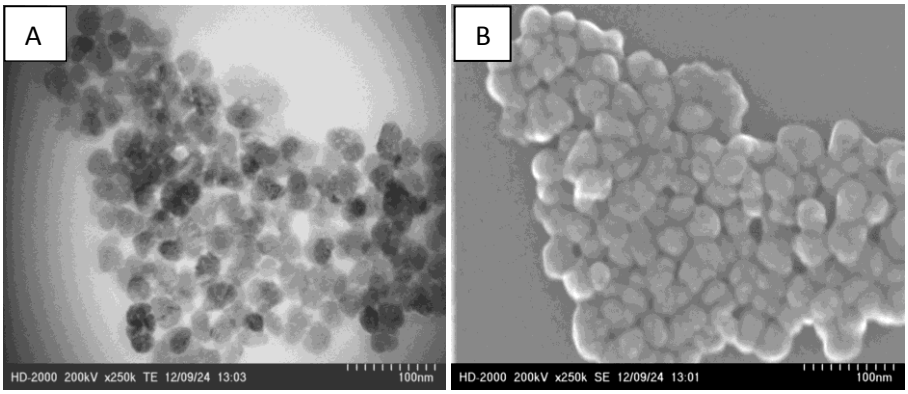

Figure 3.29. (A) TEM image and (B) SEM image of Yb:Er:$NaYF_4$-AEP nanoparticles.

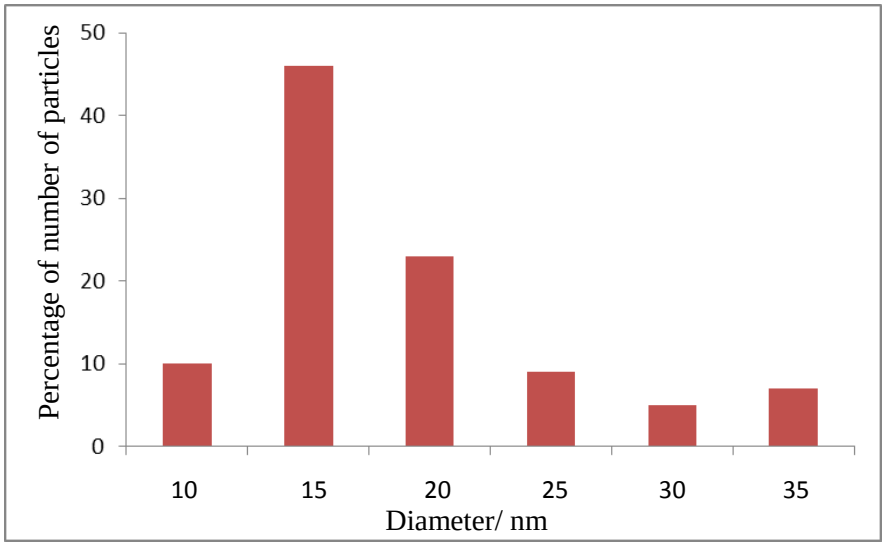

Figure 3.30. Particles diameter distribution of Yb:Er:$NaYF_4$-AEP nanoparticles obtained from the TEM image.

3.9 CONCLUSIONS

In this project, the luminescence properties, hydrophilicity, and the selectivity of nanoparticles to melanoma cancer cell-surface receptors were optimized focusing on two nanoparticle systems: europium-based down-converting nanoparticles and ytterbium-, erbium-based upconverting nanoparticles. The nanomaterials were characterized using different analytical techniques to confirm the crystal structures and the surface functionalization.

We hypothesized that the luminescence characteristics of europium-based nanoparticles could be improved by using a sensitization process. Our synthetic strategy was to functionalize the surface of the nanomaterials with a chelator ligand (namely TTA) with strong light absorption properties. We have explored two synthetic methods for introducing the TTA ligand to the nanoparticle surface. We utilized a ligand exchange method with $LaEuF_3$ nanoparticles. With the second nanoparticles system, $Eu:NaYF_4$, we modified a synthetic method to remove the pre-existing oleic acid ligands before introducing the TTA ligands.

In this work, we have confirmed that our sensitizer ligand, TTA is capable of significantly enhancing the Eu(III)-based luminescence at 614 nm upon surface functionalization of the nanoparticles. The surface modified Eu(III)-based nanoparticles with TTA ligand show characteristic light absorption in the UV region with intense luminescence as a result of the energy transfer from TTA ligand to the Eu(III)-based excited states. We have observed relatively higher quantum yield values for the smaller sized nanoparticles ($Eu:NaYF_4$, 15-20 nm) compared to those observed for large particles

($LaEuF_3$, 100-150 nm) indicating that efficient ligand-to-metal energy transfer is a distance dependent. We believe that the smaller sized nanoparticles have an optimal distance between most of the Eu(III) ions and the TTA ligand warranting an efficient energy transfer and a higher luminescence efficiency. In addition, $NaYF_4$ matrix produced highly crystalline nanoparticles compared to the low crystallinity of the LaF_3 matrix. Highly crystalline nanoparticles promise fewer crystal defects which may reduce the luminescence quenching processes. This may also contribute to the observed higher luminescence quantum yields of the $NaYF_4$ nanoparticles.

Luminescence quantum yield of the $LaEuF_3$-(AEP)-TTA nanoparticles increased with the increment of the TTA amount used for the ligand exchange process. Our TGA results confirmed a higher surface coverage of TTA with increasing the initial amount of TTA used in the ligand exchange process. Attachment of a higher amount of chromophore ligand resulted an enhanced sensitization process. This may be a reason for the increment of the observed luminescence quantum yield of the $LaEuF_3$-(AEP)-TTA nanoparticles where 32 mg of TTA was used for the ligand exchange process. However no significant increase in the luminescence quantum yield (from 32 mg of TTA) was observed when 64 mg of TTA ligand was used in the synthesis. This may be due to the surface saturation above 32 mg of TTA ligand as observed in our TGA measurements.

When $LaEuF_3$-(AEP)-TTA (using 32 mg of TTA) nanoparticle system (with a quantum yield of 4.0 %) was compared with $LaEuF_3$-(Citric acid)-TTA (32 mg of TTA) nanoparticle system, citric acid coated nanoparticles exhibited a lower quantum yield value (1.9%). Citric acid has multiple coordination sites (carboxylic groups) compared to

the single bidentate phosphate binding site of AEP. According to these structural features, citric acid may be strongly bound to the nanoparticle surface compared to AEP. Thus AEP molecules can easily be replaced by TTA ligands opposed to the strongly bound citric acid molecules during the ligand exchange process. Therefore we assume that the ligand exchange process may not be efficient with citric acid coated nanoparticles resulting a lower amount of TTA molecules on the surface of $LaEuF_3$-(Citric acid)-TTA nanoparticles. This might have reduced the sensitization efficiency resulting a lower luminescence quantum yield.

When $LaEuF_3$-(AEP)-TTA (32 mg) nanoparticle system (quantum yield of 4.0 %) was compared with $LaEuF_3$-(AEP)-HFA (32 mg) nanoparticle system, HFA coated nanoparticles exhibited a very low quantum yield value (0.78%). The electronic energy difference between the triplet level of the sensitizer ligand and the $^5D_0$ energy level of Eu(III) ion is crucial for the ligand-to-metal sensitization process.[34] The triplet level energy of the HFA ligand and the TTA ligand is at 22 000 cm^{-1} and 20 000 cm^{-1}, respectively.[34] The energy of the $^5D_0$ state of Eu(III) ion was found to be at 17 500 cm^{-1}. The energy gap between triplet state of the HFA ligand and $^5D_0$ state of Eu(III) ion is 4 500 cm^{-1}. The energy gap between TTA and $^5D_0$ state of Eu(III) ion is 2500 cm^{-1}. We believe that an energy gap of 2500 cm^{-1} may be optimum for an efficient energy transfer between the ligand and the Eu(III) ions based on our luminescence quantum yield measurements. Thus, a relatively large energy gap of 4500 cm^{-1} may reduce the sensitization efficiency in $LaEuF_3$-(AEP)-HFA nanoparticles resulting a poor luminescence quantum yield.

When Eu:$NaYF_4$-TTA nanoparticle system (with a luminescence quantum yield of 17.0 %) is compared with Eu:$NaYF_4$-btfa nanoparticle system, Eu:$NaYF_4$-btfa (32 mg) nanoparticles have a lower luminescence quantum yield (4.2%). The triplet energy of the btfa ligand is at 21 400 cm^{-1}. The energy gap between the triplet state of the btfa ligand and $^5D_0$ state of Eu(III) ion is 3900 cm^{-1}. This energy gap is larger than the energy gap between TTA ligand and Eu(III) ions (2500 cm^{-1}). Therefore the observed luminescence quantum yield of the Eu:$NaYF_4$-btfa nanoparticles are lower than that of Eu:$NaYF_4$-TTA nanoparticles.

The surface of the upconverting nanoparticles were functionalized with AEP ligand for improving the hydrophilicity. The AEP ligand was introduced after removing the preexisting oleic acid ligands using an identical synthetic strategy that we utilized for removing oleic acid in Eu:$NaYF_4$ nanoparticles. The AEP-modified nanoparticles can readily be dispersed in nanopure water (up to about 2 mg in 0.5 mL of water).

We have initialized the labeling of nanoparticles with MSH4 ligand for future *in vitro* assay studies with melanoma cells expressing human melanocortin receptors. The preliminary characterization data promises the MSH4 peptide attachment to the nanoparticle surface. Modification of the linker length between the nanoparticle surface and the peptide ligand to enhance the selectivity will be a future project. We also plan to optimize the luminescence quantum yield of the MSH4-TTA-coated nanoparticles by varying TTA / MSH4 ratio in the nanoparticles. Once fully optimized, the nanoparticles synthesized in this project have potential applications for carrying out *in vitro* and *in vivo* cell binding assays for screening of melanoma cancer targeted pharmaceuticals.

REFERENCES

1. Diamente, P. R.; Veggel, F. C. J. M. V. Water-Soluble Ln^{3+} Doped LaF_3 Nanoparticles: Retention of Strong Luminescence and Potentials as Biolabels *J. Fluor.* **2005,** *15*, 350.

2. Ferrart, M. Cancer Nanotechnology: Opportunities and Challenges *Nat. Rev. Cancer* **2005**, *5*, 161.

3. Coll, J. L. Cancer optical imaging using fluorescent nanoparticles *J. Nanomedicin*e **2012**, *6*, 7.

4. Quantum dots versus organic dyes as fluorescent labels. http://nathan.instras.com/ResearchProposalDB/doc-168.pdf (Sep 10, 2008).

5. Claude, J. G.; Bünzli1.; Svetlana, V.; Eliseeva. Lanthanide NIR luminescence for telecommunications, bio analysis and solar energy conversion *J. Rare Earths* **2010,** *28*, 824.

6. Using Synergy HT Multi-Mode Microplate Reader to Measure Time-Resolved Fluorescent Compounds. http://www.biotek.com/resources/articles/time-resolved-fluorescent-compounds.html (Oct 29, 2002).

7. De Silva, C. R.; Vagner, J.; Lynch, R.; Gillies, R. J.; Hruby, V. J. Optimization of time-resolved fluorescence assay for detection of europium-tetraazacyclododecyltetraacetic acid-labeled ligand-receptor interactions *J. Anal. Biochem.* **2009,** *398*, 15.

8. Ansari, A.; Alam, M.; Labis, P. J.; Alrokayan, S. A.; Shafi, G.; Hasan, T. N.; Syed, N. A.; Alshatwi, A. A. Luminescent mesoporous $LaVO_4$:Eu^{3+} core-shell nanoparticles: synthesis, characterization, biocompatabitlity and their cytotoxicity *J. Mater. Chem.* **2011**, *10*, 1039.

9. Song, Y.; Tian. Q.; Zou, R.; Chen, Z.; Yang, J.; Hu, J. Phase and luminescent intensity control of hydrophilic rare-earth up-converting nanophosphors prepared by one-pot solvothermal synthesis *J. Alloys Compd.* **2011**, *509*, 6539.

10. Nyk, M.; Kumar, R.; Ohulchanskyy, T. Y.; Bergey, E. J.; Prasad, P. N. High Contrast *in vitro* and *in vivo* Photoluminescence bioimaging Using Near Infrared to Near Infrared Up-Conversion in Tm^{3+} and Yb^{3+} Doped fluoride Nanophosphors *Nano Lett*. **2008**, *8*, 11.

11. Loic, J.; Charbonniere, L. J.; Rehspringer, J. L.; Ziessel, R.; Zimmermann, Y. Highly luminescent water-soluble lanthanide nanoparticles through surface coating sensitization *New J. Chem.* **2008,** *32*, 1055.

12. Ong, L. C.; Gnanasammandhan, M. K.; Nagrajan, S.; Zhang, Y. Upconversion: road to EI Dorado of the fluorescence world *J. Bio. Chem. Lumi*. **2010**, *25*, 290.

13. Mai, H.; Zhang, Y.; Si, R.; Yan, Z.; Sun, L.; You, L.; Yan, C. High-Quality Sodium Rare-Earth Nanocrystals: Controlled Synthesis and Optical Properties *J. Am. Chem. Soc.* **2006**, *128*, 1636.

14. Wang, M.; Abbineni, G.; Clevenger, A.; Mao, C.; Xu, S.; Upconversion Nanoparticles: Synthesis, Surface Modification, and Biological Application *Nanomedicine* **2011**, *7*, 710.

15. Heather, L.; Handl, R. J.; Gillies, T. Lanthanide-luminescent assays for ligand receptor interactions *Life Sci.* **2004**, *77*, 361.

16. Wang, F.; Banerjee, D.; Liu, Y.; Chenc X.; Liu, X. Upconversion nanoparticles in biological labeling, imaging, and therapy *Analyst* **2010**, *135*, 1839.

17. Periodic Table of Elements. http://www.radiochemistry.org/periodictable/la_series /L9.html. (Nov 20, 2003).

18. Ruoxue, Y.; Yadong, L. Down/Up Conversion in Ln^{3+}-Doped YF_3 Nanocrystals *Adv. Funct. Mater*. **2005**, *15*, 76.

19. Kattela, J. K.; Parka, Y.; Xua, W.; Kima, G. H,; Leea, E. J.; Bonya, B. A.; Heoa, W. C.; Changb, Y.; Kimc, T. J.; Dod, J. Y.; Chaed, K. S.; Kwaka, Y. W.; Leea, G. H. Water soluble ultrasmall Eu_2O_3 nanoparticles as a fluorescent imaging agent: *In vitro* and *in vivo* studies *Colloids and Surfaces* **2012**, *394*, 85.

20. Ramirez, A.; Knope, K.; Kelley, T.; Grieg, N.; Einkauf, J.; Lill, D. Structure and luminescence of a 2-dimensional 2,3-pyridinedicarboxylate coordination polymer constructed from lanthanide(III) dimmers *Inorg. Chim. Act*. **2012**, *392*, 46.

21. Raymond Group Research. http://www.cchem.berkeley.edu/knrgrp/ln.html. (Jan 02, 2013).

22. Binnemans, K. Lanthanide-Based Luminescent Hybrid Materials *Chem. Rev.* **2009,** *109,* 4283.

23. De Silva, C. R.; Maeyer, J. R.; Wang, R.; Nichol, G. S.; Zheng, Z. Adducts of europium β-diketonates with nitrogen *p,p'*-disubstituted bipyridine and phenanthroline ligands: Synthesis, structural characterization, and luminescence studies *Inorg. Chim. Act*. **2007**, *360*, 3543.

24. Bogdan, N.; Vetrone, F.; Ozin, G.; Caobianco, J. Synthesis of Ligand-Free Colloidally Stable Water Dispersible Brightly Luminescent lanthanide-Doped Upconverting Nanoparticles *Nano Lett*. **2011**, *11*, 835.

25. Malek, Z. A. A. Melanocortin receptors: their functions and regulation by physical agonists and antagonists *Cell Mol. Life Sci*. **2001**, *58*, 434.

26. Monshi, A.; Foroughi, M.; Monshi, M. Modified Scherrer Equation to Estimate More Accurately Nano-Crystallite Size Using XRD *World Journal of Nano Science and Engineering* **2012**, *2*, 154.

27. Putting Cell Size in Perspective. http://flowingdata.com/2009/10/30/putting-cell-size-in-perspective/. (Oct 30, 2009).

28. Chen, J.; Zhao, J. X. Upconversion Nanomaterials: Synthesis, Mechanism, and Applications in Sensing *Sensors* **2012,** *12*, 2414.

29. Naccache, R.; Rodriguez, E. M.; Bogdan, N.; Rodriguez, F. S.; Cruz, M. C. I.; Fuente, A. J.; Vetrone, F.; Jacque, D.; Sole, J. G.; Capobianco, J. A. High Resolution Fluorescence Imaging Cancers Using Lanthanide Ion-Doped Upconverting Nanocrystals *Cancers* **2012**, *4*, 1067.

30. Wang, X.; Zhuang, J.; Peng, Q.; Li, Y. D. Hydrothermal Synthesis of rare-earth fluoride nanocrystals. *Inorg. Chem*. **2006**, *45*, 6661.

31. Li, H. A.; Lu, Q. Power-dependent upconversion intensity in $NaYF_4$, Yb^{3+}, Er^{3+} nanoparticles. *Inorg. Chem*. **2011**, *96*, 18001.

32. Lifetime Data of Selected Fluorophores. http://www.iss.com/resources/reference /data_tables/LifetimeDataFluorophores.html. (Jan 30, 2013).

33. Geochemical Instrumentation and Analysis. http://serc.carleton.edu/ research education/geochemsheets/eds.html. (Jul 23, 2012).

34. Klink, S. I.; Hebbink, G.; Grave, L.; Alink, P.; Van Veggel, F.; Werts, M. Synergistic Complexation of Eu^{3+} by a Polydentate Ligand and a Bidentate Antenna to Obtain Ternary Complexes with High Luminescence Quantum Yields. *J. Phys. Chem A*. **2002,** *106*, 3681.